Plant-Wide Modeling, Optimization and Control of an Industrial Diesel Hydroprocessing Plant

by

Erdal Aydın

A Thesis Submitted to the

Graduate School of Sciences and Engineering

in Partial Fulfillment of the Requirements for

the Degree of

Master of Science

in

Chemical and Biological Engineering

Koc University

September 2015

Koc University

Graduate School of Sciences and Engineering

This is to certify that I have examined this copy of a master's thesis by

Erdal Aydın

and have found that it is complete and satisfactory in all respects,

and that any and all revisions required by the final

examining committee have been made.

Committee Members:

_____

Yaman Arkun, Ph. D. (Advisor)

_____

Alper Uzun, Ph. D.

_____

Serkan Kıncal, Ph. D.

Date: _____

To my family and Burcu

ABSTRACT

Diesel hydroprocessing is an important refinery process which consists of hydrodesulfurization to remove the undesired sulfur from the oil feedstock followed by hydrocracking and fractionation to obtain diesel with desired properties. Due to the new emission standards to improve the air quality, there is an increasing demand for the production of ultra low sulfur diesel fuel. The first of the thesis is addressing the development of a reliable dynamic process model which can be used for real-time optimization and control purposes to improve the process conditions of existing plants to meet the low-sulfur demand. The overall plant model consists of a hydrodesulfurization (HDS) model for the first two reactor beds followed by a hydrocracking (HC) model for the last cracking bed. The models are dynamic, non-isothermal, pseudo-homogeneous plug flow reactor models. Reaction kinetics are modeled using the method of continuous lumping which treats the reaction medium as a continuum of species whose reactivities depend on the true boiling point of the mixture. The key modeling parameters are estimated using industrial data. Steady-state and dynamic model predictions of the reactor bed temperatures, sulfur removal, and diesel production match closely the plant data.

The industrial Diesel Hydroprocessing plant operates with varying feed-stocks and large throughputs. Also, changing market conditions have significant effects on the diesel product specifications. In the presence of such a dynamic environment, the DHP plant has to run in the most profitable and safe way while satisfy the product requirements and not violating specified constraints. In the second part of the thesis, a hierarchical, cascaded model predictive control structure is proposed to be used for real-time optimization of the industrial DHP plant using developed models. The performance of the control structure is checked with closed loop simulations for both set point tracking and disturbance rejection cases.

ÖZET

Dizel hidro-işlemesi, içinde sülfür giderimi için hidrodesülfürizasyon ve istenen dizel ürünün elde edilmesi için hidrokraking ve ayrıştırma işlemlerini bulunduran önemli bir rafineri sürecidir. Hava kirliliği ve küresel ısınma etkilerinin azaltılması yönünde belirlenen yeni salınım kuralları ile birlikte, çok düşük kükürt seviyeli dizel üretimine duyulan ilgi artmıştır. Bu tezin ilk kısmında, çok düşük kükürt seviyeli dizel üretilen rafinerilerin, dinamik süreçlerinin modellemesi için kullanılabilecek güvenilir modellerin elde edilme çalışması yapılmıştır. Çalışmanın yapıldığı rafineri ünitesinde, iki adet hidrodesülfürizasyon ve bir adet hidrokraker reaktörleri birbirine seri bağlı şekilde çalıştırılmaktadır. Tasarlanan modeller dinamik, eş-ısıl olmayan, sözde-homojen, integro-diferansiyel ve tapa akış reaktör modelleridir. Reaksiyon kinetikleri sürekli kümeleme yöntemi kullanılarak modellenmiştir. Sürkeli kümeleme yönteminde, tepkin karışımların tepkime özellikleri gerçek kaynama noktalarına göre tayin edilir. Önemli model değişkenleri, gerçek ünite ölçümleri kullanılarak belirlenmiştir. Değişken ve yatışkan haldeki sıcaklık, sülfür giderimi ve dizel üretimi model öngörü sonuçları ünite ile yakın derecede uyumludur.

Endüstriyel dizel hidro-işleme üniteleri yüksek derecede değişkenlik gösteren beslemeler ve yüksek akış hızlı ürün çıktıları ile çalıştırılmaktadır. Ayrıca, pazardaki değişkenlikler dizel ürünü gereklilikleri üzerinde önemli etkilere sahiptir. Bu nedenle, dizel hidro-işleme ünitelerinin güvenli, kısıtları aşmayaca ve karlılık oranı en yüksek şekilde sürdürülmesi büyük önem arz etmektedir. Bu tezin ikinci kısmında, elde edilen ünite modelleri kullanılarak, endüstriyel dizel hidro-işleme üniteleri için eş-zamanlı en-iyileme ve kademeli kontrol sistemi tasarlanmıştır. Tasarlanan kontrol sistemi iki katmanlı ve kademelidir. Bu kontrol sisteminin üst kademesi karlılık hedefli çalışırken, alt kademesi bağımsız kontrol yapılarını koordine eder. Tasarlanan kontrol sisteminin performansı, kapalı döngü hedef değere ulaşma ve bozucu etki giderme simülasyonları ile denetlenmiştir.

ACKNOWLEDGEMENTS

Firstly, it gives me a great pleasure to express my gratitude to my advisor Prof. Dr. Yaman Arkun for allowing me to work on this project, for his support, patience, inspiration and immense knowledge. His door was always open to me for sharing his ideas and discussing.

Besides my advisor, I would like to thank the rest of my thesis committe: Asst. Prof. Dr. Alper Uzun and Asst. Prof. Dr. Serkan Kıncal, for accepting to be in the committe and for their insightful comments and encouragements.

My sincere thanks goes to my project partner Ayse Dilan Çelebi and Dr. Hasan Şıldır for their success and clearness in their past studies, for being eager to share their ideas with me, and most importantly for their support. Dr. Şıldır was always there for answering my questions even though he was doing his military service. His contribution to this project is very significant. I feel very lucky for being partners and friends with such great individuals.

I would like to thank the Tüpraş R&D Department, espacially to Gamze İş and Ümmühan Canan, for the great hospitality during our visits to the refinery and willingness to share information and knowledge in this project. I would also like to thank to Mustafa Mutlu and Murat Erdoğan for their valuable comments and suggestions.

The research scholarship and housing from Koc University Foundation are acknowledged. I also thank all my professors in the Middle East Technical University for the education and support they offer throughout my undergraduate years.

I want to thank my father İsmet Aydın for his effort for me to get a good education throughout his life. My whole family always support me. I feel myself blessed for having them in my life.

Lastly, I want to show my gratefulness to the secret hero of my life, my beloved Burcu, for her infinite support, patience and encouragements.

TABLE OF CONTENTS

LIST OF TABLES

LIST OF FIGURES

NOMENCLATURE

T = Bed temperature (K).

T_0 = Reference temperature (K).

TBP = True Boiling Point (^{0}C).

$TBP(h)$ = Highest boiling point (^{0}C).

$TBP(l)$ = Lowest boiling point (^{0}C).

C_p = Heat capacity (kJ/kg-K).

ΔT = Bed temperature difference (^{0}C).

v =Average velocity (m/h).

$C(t)$ = Concentration (kg/kg-feed).

$c(k,0,0)$ = Initial oncentration of species at the reactor inlet (kg/kg-feed).

$k_{\min 1}$ = Minimum reactivity of sulfur species in Bed 1 (h^{-1}).

$k_{\min 2}$ = Maximum reactivity of sulfur species in Bed 2 (h^{-1}).

k = Reactivity (h^{-1}).

$D(k)$ = Species type distribution function.

$k_{\max 1}$ = Maximum reactivity of sulfur species in Bed 2 (h^{-1}).

$k_{\max 2}$ = Maximum reactivity of sulfur species in Bed 2 (h^{-1}).

wt = Weight fraction.

K = Maximum reactivity in the hydrocracker (h^{-1}).

N = Number of sulfur species.

E_{a1} = Activation energy in Bed 1 (kJ/kmol).

E_{a2} = Activation energy in Bed 2 (kJ/kmol).

ΔH_1 = Heat of reaction in Bed 1 (kJ/kg-sulfur).

ΔH_2 = Heat of reaction in Bed 2 (kJ/kg-sulfur).

$k_{hc,\max}$ = Maximum reactivity of hydrocarbon species in the the hydrocracker bed (h^{-1}).

$E_{a,hc}$ = Activation energy for the hydrocracking reactions (kJ/kmol).

c = Parameter for the heat of cracking reaction.

d = Parameter for the heat of cracking reaction.

TCP = Temperature cut point.

a_i = Blending parameter for heavy diesel.

b_i = Blending parameter for light diesel.

c_i = Blending parameter for light vacuum gas oil.

d_i = Blending parameter for imported diesel.

$D86^{HD}$ = ASTM D86 values of heavy diesel. (^{0}C)

$D86^{LD}$ = ASTM D86 values of light diesel. (^{0}C)

$D86^{LVGO}$ = ASTM D86 values of light vacuum gas oil. (^{0}C)

$D86^{Im.Diesel}$ = ASTM D86 values of imported diesel. (^{0}C)

$D86^{FEED}$ = ASTM D86 values of DHP Feed Drum. (^{0}C)

S_f = Feed sulfur weight percent. (%)

F_f = Feed flow rate (ton/day)

m_{Tank} = Total mass in the blending tank. (ton)

τ_{tank} = Time constant of blending tank.

x_{HD} = Mass fraction of heavy diesel.

$Feed\ T^{95}$ = The temperature at which 95 % of DHP Feed by volume boils. (^{0}C)

$Diesel\ T^{95}$ = The temperature at which 95 % of Diesel by volume boils. (^{0}C)

$Sconv$ = Conversion of sulfur.

M_{HD} = Flow rate of heavy diesel. (ton/day)

M_{LD} = Flow rate of light diesel. (ton/day)

$M_{\mathrm{ImportDiesel}}$ = Flow rate of import diesel. (ton/day)

$T_{in,HDS1}$ = Inlet Temperature of the first HDS reactor. (K)

$T_{in,HDS2}$ = Inlet Temperature of the second HDS reactor. (K)

$T_{in,HC}$ = Inlet Temperature of the HC reactor. (K)

$T_{out,HDS1}$ = Outlet Temperature of the first HDS reactor. (K)

$T_{out,HDS2}$ = Outlet Temperature of the second HDS reactor. (K)

$T_{out,HC}$ = Outlet Temperature of the HC reactor. (K)

C_{HD} = Cost of heavy diesel.

C_{LD} = Cost of light diesel.

$C_{ImportDiesel}$ = Cost of import diesel.

P_{Diesel} = Price of product diesel.

P_{Nafta} = Price of product nafta.

sp=set point.

θ = Normalized boiling point.

α = The parameter that relates cracking reactivity to normalized boiling point.

α_0 = The parameter in the yield function.

α_1 = The parameter in the yield function.

β = The parameter that relates HDS reactivity to the normalized boiling point.

Chapter 1

INTRODUCTION

Diesel is a petroleum fossil fuel that contains different forms of sulfur compounds including mercaptans, sulfides, disulfides, thiophenes, benzothiophenes, dibenzothiophenes, and substituted dibenzothiophenes. Combustion of sulfur compounds in diesel engines emits sulfur oxides into the atmosphere, which can cause detrimental effects on the human health and the environment. In order to comply with the new emission standards to improve the air quality, there is an increasing demand for the production of ultra low sulfur diesel (ULSD) fuel (<10 ppm). In the future, this trend towards "zero" sulfur diesel is expected to continue [1]. In order to meet the low-sulfur demand, refineries are considering alternative revamping strategies such as design changes, new catalysts and improvements in process [2]. In parallel with increasing market demand for low sulfur diesel, research in the production of ULSD has gained increased popularity in the scientific community [1].

The industrial hydro-processing plant subject to this study consists of two catalytic hydro-desulfurization (HDS) reactors and a hydro-cracking (HC) reactor in. The feedstock of the unit is a blend of four streams: HD (straight run heavy diesel), LD (straight run light diesel), LVGO (light vacuum gas oil) and an imported diesel. HD and LD streams are obtained from a crude distillation unit, and LVGO stream is derived from a vacuum distillation unit. These streams are blended in order to obtain a desired T95 value for the reactor feed. In the first two HDS beds, the organic sulfur impurities are removed. Hydrocracking (HC) occurs in the last bed where heavier hydrocarbons are cracked to lower molecular weight petroleum fractions. Inter-stage cooling by quench hydrogen is used in both reactors to control the bed exit temperatures. Reactor effluent is next fed to the separation unit where end products naphtha and diesel are obtained.

The industrial diesel hydro-processing plant operates with varying feedstocks and large throughputs. Also, changing market conditions have significant effects on product specifications. Therefore, slight improvements on process conditions may result in high profit

increases. In such a dynamic environment, the diesel hydroprocessing plant must be processed in the most profitable and safe way. The main operational objectives are to maximize the overall profit of the plant and to keep the sulfur content of diesel below 10 ppm. Therefore, optimum steady-state operating conditions have to be calculated using an economic objective function, and a proper control configuration has to be designed.

In Chapter 2, the focus is on the steady and dynamic modeling studies of the plant using continuous lumping approach. Non-linear first principle models are obtained and these models are trained with real industrial plant data using parameter estimation techniques. The prediction results match the plant data closely.

In Chapter 3, a hierarchical cascaded model predictive control structure is proposed along with the plant-wide optimization structure for the DHP plant. In addition, for the feed blending and the fractionation units, new empirical models are developed to predict certain important feed and product properties for optimization and control purposes. The main task of the cascaded MPC structure is to coordinate the decentralized regulatory blending and reactors MPCs together to reach the plant wide optimal operating point.

Chapter 2

DYNAMIC MODELING OF THE DIESEL HYDROPROCESSING PLANT

2.1 Introduction

The simplified flowsheet for the industrial diesel hydroprocessing (DHP) plant is shown in Figure 2.1. The plant is designed to process 4500 cubic meters per day of diesel feedstock. The process consists of a blending section followed by three catalytic reactor beds which consist of two hydrodesulfurization (HDS) and one hydrocracking (HC) bed. The feed is obtained by blending four streams: HD (straight run heavy diesel), LD (straight run light diesel), LVGO (light vacuum gas oil) and an imported diesel. HD and LD streams are derived from a crude distillation unit, and LVGO stream is derived from another vacuum distillation unit. Imported diesel's specifications are close to the product specifications of the DHP Plant except the sulfur content. It is used as an additive in order to keep the product T95 value (the temperature at which 95% of the distillate is collected e.g. by ASTM D86 distillation) at desired specifications. These streams are blended in order to obtain a desired T95 value for the reactor charge. The blended feed is mixed with the recycle hydrogen gas (treat gas) before it enters the furnace where it is heated to the required reactor inlet temperature. Hydrodesulfurization occurs at high temperatures in the presence of excess hydrogen to produce higher-value hydrocarbon products with lower sulfur levels. In the first two catalytic HDS beds (usually with $CoMo/Al_2O_3$ or $NiMo/Al_2O_3$ catalysts), the organic sulfur compounds are converted to hydrogen sulfide. Reactors operate at high pressures (3.0–5.0 MPa) and temperatures (300–450 $^{\circ}$C). Hydrogenation reactions are exothermic; therefore, reaction products are cooled by the hydrogen quench flows between beds. Hydrocracking (HC) occurs in the third bed in which the high-boiling, high molecular weight hydrocarbons crack to lower-boiling point species. The last (fourth) bed is used for dewaxing to improve the cold flow properties during winter operation. The presented model does not include this bed since it covers the days of summer diesel operation when the last bed was inactive. HDS and HC units are trickle bed reactors in which the liquid phase consists of the heavy gas oil feed;

hydrogen is in the gas phase and the catalyst constitutes the solid phase. The HC product is separated into the end products which are the diesel and the naphta. Important product specifications are the sulfur content and T95 value for the diesel.

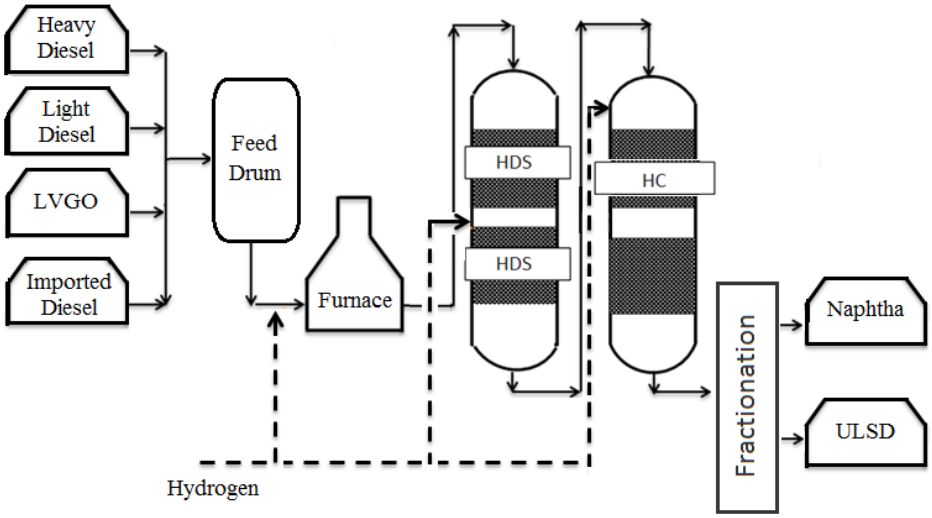

Figure 2.1: Simplified DHP plant flowsheet.

The kinetics of hydrodesulfurization is complex since the diesel feedstock contains a variety of organic sulfur compounds. In general, the difficulty of sulfur removal increases in the order: paraffins < naphthenes < aromatics [3]. Reactivities of different sulfur compounds depend on their boiling points as shown in Figure 2.2 [4]. For treating oil to lower and lower sulfur levels, it is necessary to remove sulfur from the heavier hydrocarbon fractions that are the most difficult to desulfurize. As shown in Figure 2.2 [4], the higher molecular weight dibenzothiophenes are sterically hindered refractive compounds that are the most difficult to treat.

Typical HDS reactions are shown in Figure 2.3 [5]. Mechanistic kinetic modeling of hydrodesulfurization is a challenging task because of the large number of compounds participating in many complex reactions. In this work we use the continuous lumping method that considers the reactive mixture as a continuum [6],[7]. Continuous lumped models are relatively easy to develop, and they have fewer number of modeling parameters to estimate. At the same time they are known to possess good predictive capabilities [8].

Eventually, we want to use the developed model for optimization and control of the industrial unit. For this reason, the model should be able to predict both the steady-state and

dynamic behavior of the actual process. At the same time, while capturing the essential features of the industrial process, unnecessary details which can hinder its end use must be avoided. Therefore, in this work, instead of an heterogeneous multi-dimensional model, we choose to develop a pseudo-homogeneous, one-dimensional dynamic reactor model. Similarly, instead of a more detailed mechanistic kinetics modeling, we use a kinetic model based on continuous lumping.

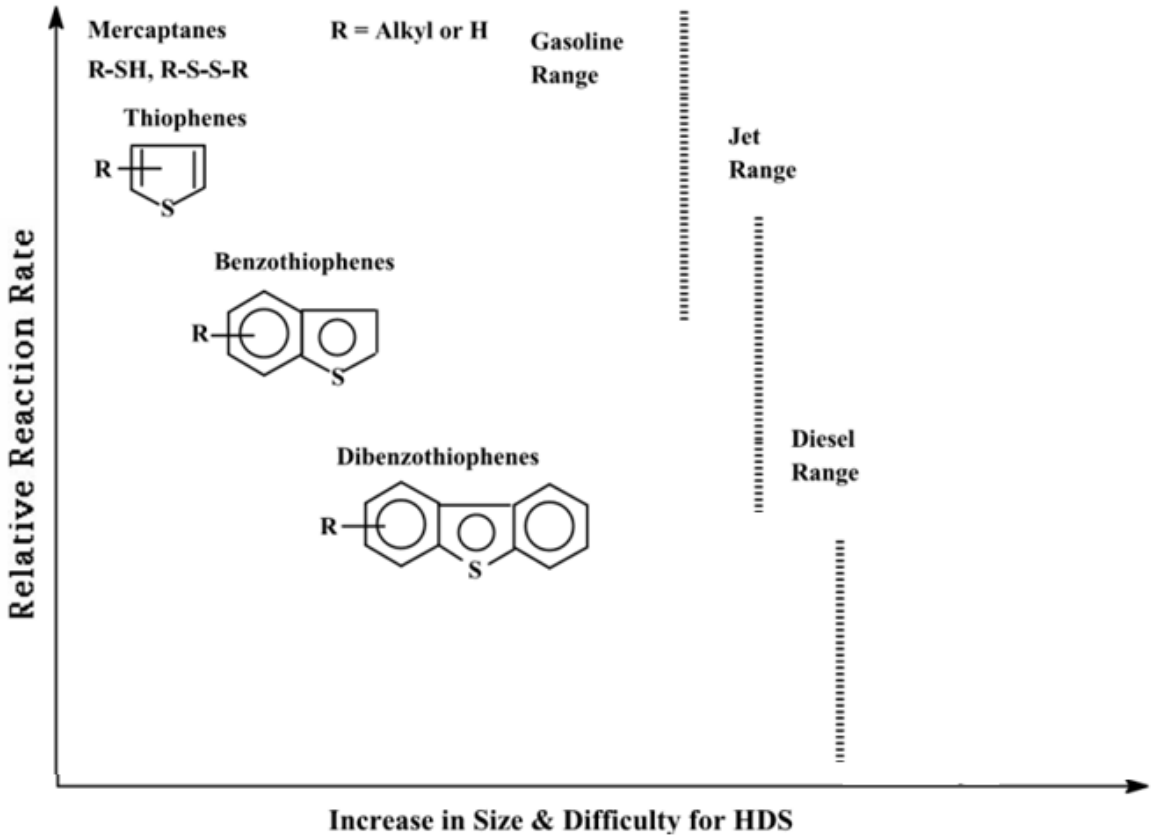

Figure 2.2. Reactivities of sulfur compounds.

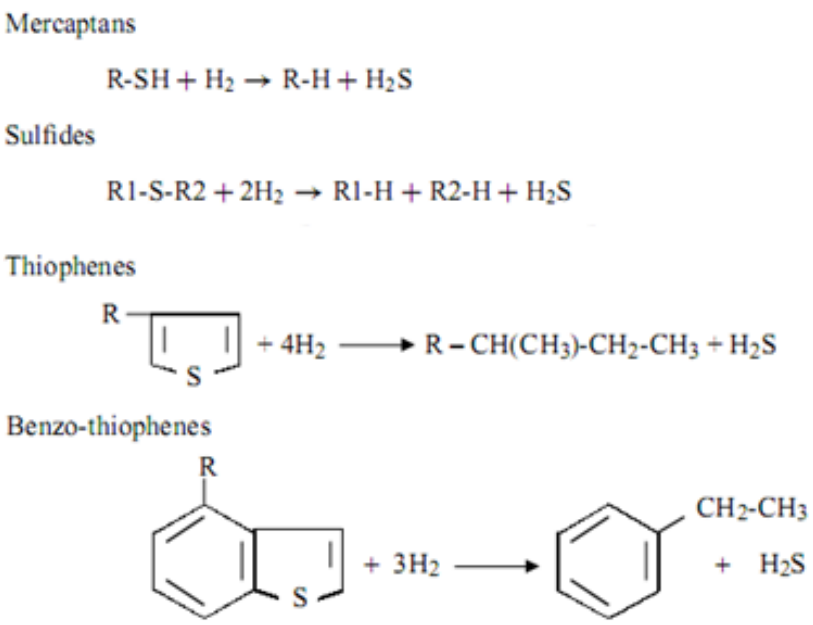

Figure 2.3. Some of the HDS reactions.

2.2 Modeling Studies

2.2.1 Mathematical Preliminaries for Continuous Lumping

For a mixture that has N reactant species, the total concentration at time t is given by

$$C(t) = \sum_{i=1}^{N} c_i(t) \tag{2.1}$$

where $c_i(t)$ is the concentration of the i^{th} reactant and $C(t)$ is the total concentration. In our case for the HDS beds, the reactant is the sulfur compound.

In Chou and Ho [7] , the above discrete mixture was approximated by a continuous mixture where the concentrations are continuous functions of reactivity *k*. This is achieved by a coordinate transformation from discrete "*i*-coordinate" to continuous "*k*-coordinate" given by:

$$D(k_i) = \frac{\Delta i}{\Delta k_i} \tag{2.2}$$

As the number of species N approaches infinity, $D(k_i)$ becomes a continuous function of k and $D(k)dk$ represents the number of species with reactivity between k and $k+dk$. With these definitions, one gets the continuous representation of the discrete mixture:

$$C(t) = \int_0^\infty c(k,t)D(k)dk \tag{2.3}$$

where *c(k,t)* is the concentration of reactant with reactivity *k* at time *t* in the continuous mixture. *D(k)* is known as the species-type distribution function.

The literature suggests that for HDS reactions, the reactivity of sulfur species decreases monotonically with the True Boiling Point (TBP). Accordingly, the following relationship has been used to model this dependency [9]:

$$k = k_{\min} - k_{\max} \ln[e^{-1} - (e^{-1} - 1)\theta^{\frac{1}{\beta}}] \tag{2.4}$$

where $k_{\min}$, $k_{\max}$ and β are adjustable (to be estimated) parameters and variable θ is the normalized true boiling point. Figure 2.5 shows how the reactivity of different sulfur compounds changes as a function of the the boiling point according to Eq. 2.4.

The normalized true boiling point θ is defined by:

$$\theta = \frac{TBP - \min(TBP)}{\max(TBP) - \min(TBP)} \tag{2.5}$$

The distribution function is determined from its definition:

$$D(k) = \frac{di}{d\theta}\frac{d\theta}{dk} = N\frac{d\theta}{dk} \tag{2.6}$$

where $\frac{d\theta}{dk}$ is computed from Eq. 2.4. It is this form of sulfur species-type distribution function $D(k)$ that has been used in all of the HDS continuous lumping models in the literature.

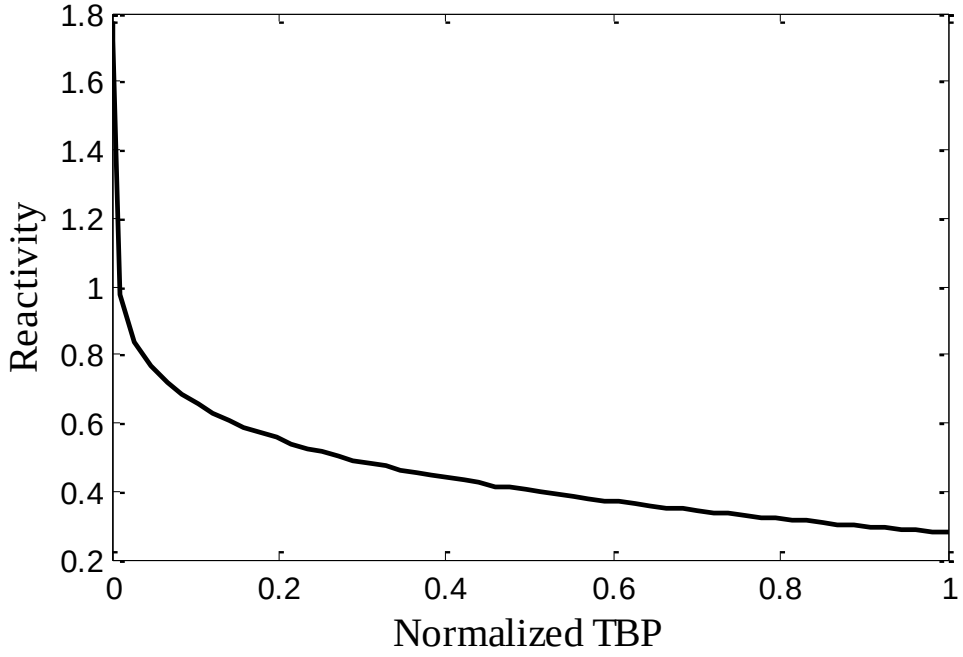

Figure 2.4. Hydrodesulfurization rate constant versus TBP.

As seen from Figure 2.4, the most reactive sulfur compounds are those present in light fractions and the least reactive ones are the most refractive compounds present in heavy fractions.

2.2.2 HDS Reactor Model

HDS units are trickle bed reactors in which the liquid phase consists of blended gas oil feed; hydrogen is in the gas phase and the catalyst constitutes the solid phase. Froment et al. [10] developed a one–dimensional heterogeneous non-isothermal model for a feed mixture that consisted of benzothiophene, dibenzothiophene and alkyl-substituted DBTs. A three-phase reactor model was developed by Korsten and Hoffman [11] simulate a pilot trickle-bed

reactor in which the hydrotreating reaction of vacuum gas oil took place under high–pressure and isothermal conditions. The model assumed a two–film theory where mass transfer coefficients and the physical properties were estimated by correlations. Bhaskar et al. [12] developed a three phase heterogeneous model including mass transfer at the gas-liquid and the liquid-solid interfaes and applied it to a pilot plant trickle–bed reactor which had an atmospheric gas oil feed. Chowdhury et al. [13] developed a two phase flow reactor model for desulfurization and dearomatization of diesel oil in an experimental trickle- bed reactor.

Due to more stringent restrictions on sulfur, HDS reactor operation is requiring tighter control to meet these specifications. The HDS reactors should be able to process varying quality oil feeds and be able to respond to changing market demands. Therefore, there is an increasing need for the development of dynamic models that can reliably predict the performance of HDS reactors under different operating conditions. Such a model would be useful for diagnostics, improving process understanding, operator training, and real-time control. In fact, in this work, the dynamic HDS model has been developed for a real-time optimization and control project for the refinery.

Pseudo-homogeneous models neglecting mass and heat transfer resistances have been widely reported in the literature due to their reliability and simplicity. Sau et al. [14] proposed a pseudo-homogeneous plug-flow model and simulated a commercial kero-HDS reactor by applying the continuum lumping theory. They grouped organic sulfur compounds into different classes: mercaptans, sulfides, disulfides, and thiophenes. Langmuir-Hinshelwood kinetics including the inhibiting effect of hydrogen sulfide was used. A continuous kinetic model for an industrial hydrocracking reactor was developed by Basak et al. [15]. The hydrogen consumption and bed temperature profiles were simulated. Sertic-Bionda et al. [16] developed a simple steady-state pseudo-homogeneous plug-flow model to simulate a trickle bed reactor for the hydrotreatment of atmospheric gas oil and light cycle oil.

Relative to the steady-state models, there are not many dynamic models for HDS reactors in the open literature. Mahinsa et al. [17] presented a pseudo-homogeneous two-dimensional dynamic model with axial convection and radial dispersion of mass. Results showed negligible radial effects and one-dimensional modeling was recommended. Mederos et al. [18], [19] developed a heterogeneous one-dimensional model that consisted of dynamic mass and energy balance equations for the liquid and solid phases. All the reactions of different sulfur compounds were lumped to a single HDS reaction. A heterogeneous transient,

non-isothermal fixed bed model was considered in [20]. Only desulfurization of thiophene was simulated to reduce the computations. In Chen et al. [21] a dynamic two-dimensional hydrotreater model with axial and radial dispersion of heat and mass is given. Hydrotreatment of a partially stabilized light-coker naphtha was studied and the heat effects related to all of the chemical reactions were associated with a single olefin hydrogenation reaction.

In the present work, the used model is a single-phase (liquid) pseudo-homogeneous one-dimensional plug flow reactor model with a kinetic model that uses continuous lumping. As such, in addition to the steady-state behavior, it can also predict the dynamic response of the reactor. Although the developed model bears some similarities with the existing steady-state models, this is the first pseudo-homogeneous, one dimensional HDS reactor model that treats both dynamics and continuous lumping together to the best of our knowledge.

In the model the heat and mass transfer resistances between phases are assumed negligible. Temperature and concentrations change only as a function of time and axial position in the bed. Hydrodesulfurization product H_2S is reported to inhibit the reaction kinetics in the literature [9, 18, 19]. However, since there is no way of independently verifying it in the plant, it was assumed that there is no H_2S inhibition. It is further assumed that catalyst deactivation is relatively slow and catalyst activity does not change during the period the data is collected. Any possible H_2S inhibition or catalyst deactivation effects are indirectly accounted for by the rate constant estimated from plant data. It is also assumed that hydrogen is in excess and reactions can be modeled by first order kinetics. With these assumptions, taking a differential reactor volume, the unsteady-state differential mass balance for the plug flow reactor can be written as follows:

$$F_s\big|_V - F_s\big|_{V+\Delta V} + r\Delta V = \frac{dN_s}{dt} \tag{2.7}$$

where N_s represents the number of moles of sulfur species, *r* is the reaction rate and $F_{s,in}$ and $F_{s,out}$ are the inlet and outlet flow rates of the sulfur species into and out of the differential volume element. Eq. 2.7 can be re-written as:

$$C_s\big|_z A_c \nu - C_s\big|_{z+dz} A_c \nu - k C_s A_c dz = \frac{d(A_c dz C_s)}{dt} \tag{2.8}$$

where A_c is reactor cross-sectional area, v is the average velocity, k is the reaction rate and C_s is the concentration of sulfur species. Dividing each term by $A_c dz$ and taking limit as dz approaches to zero, Eq. 2.8 becomes:

$$-v\frac{\partial C_s(k,z,t)}{\partial z} - kC_s(k,z,t) = \frac{\partial (C_s(k,z,t))}{\partial t} \tag{2.9}$$

Modifying Eq. 2.9 by dividing to total concentration and relating the reaction rate by the hydrodesulfurization reaction equation (Eq. 2.4) and also by using Arrhenius type relation in order to take into account the non-isothermal behaviour, the final mass balance equation can be obtained as follows:

$$\frac{\partial w(k,z,t)}{\partial t} = -v\frac{\partial w(k,z,t)}{\partial z} - k_0 e^{\frac{-E_a}{R}\left(\frac{1}{T}-\frac{1}{T_0}\right)} w(k,z,t) \tag{2.10}$$

where $w(k,z,t)$ is the sulfur mass fraction of the compound with reactivity k at position z and time t. E_a is the activation energy; k_0 is the rate constant at some reference temperature T_0. Once Eq. 2.10 is solved, the total weight fraction of the sulfur within the TBP range θ_1- θ_2 or the corresponding reactivity k_1-k_2 can be determined from:

$$w_{1,2} = \int_{k_1}^{k_2} w(k,z,t)D(k)dk \tag{2.11}$$

Unsteady-state energy balance is similarly derived as:

$$\rho A_c v C_p (T(z,t)\big|_z - T(z,t)\big|_{z+dz}) + \rho A_c dz \int_0^{k_{\max}} k w(k,z,t)D(k)(-\Delta H_r(k))dk = \rho A_c C_p (\frac{\partial T(z,t)}{\partial t}) \tag{2.12}$$

where C_p is the specific heat capacity of the feed; and $\Delta H_r(k)$ is the heat of desulfurization reaction for the species with reactivity k.

Arranging Eq. 2.12, the energy balance equation can be obtained as follows:

$$\frac{\partial T(z,t)}{\partial t} = -v\frac{\partial T(z,t)}{\partial z} + \frac{1}{C_p}\int_0^{k_{\max}} k_0 e^{\frac{-E_a}{R}\left(\frac{1}{T}-\frac{1}{T_0}\right)} w(k,z,t)D(k)(-\Delta H_r(k))dk \quad (2.13)$$

For simplicity a constant average values for $\Delta H_r(k)$ have been used. The second term on the right hand side of Equation 2.13 is a sum of the heat of reactions due to all types of sulfur species undergoing hydrodesulfurization. In particular $w(k,z,t)D(k)dk$ denotes the total mass fraction of sulfur with reactivity between *k* and *k+dk* that reacts.

In order to solve the integro-differential reactor equations Eq. 2.10 and 2.13, one needs to specify the initial sulfur distribution of the feed i.e. $w(k,0,0)$. In order to compute $w(k,0,0)$, the oil feed is divided into *N* pseudo-components where each pseudo-component boils in a particular temperature range and contributes to the feed by its weight fraction given by:

$$w_i = \int_{k_{i-1}}^{k_i} w(k,0,0)D(k)dk \qquad for \quad i = 1.2.,,,.N. \quad (2.14)$$

When the weight fraction of sulfur in the feed i.e. w_i is available from the plant measurements, $w(k,0,0)$ can be obtained by inverting Eq. 2.13 subject to the constraint:

$$\sum_{i=1}^{N} w_i = 1 = \int_0^{k_{\max}} w(k,0,0)D(k)dk \quad (2.15)$$

Using the calculated $w(k,0,0)$ and the known value of the reactor inlet temperature *T(0,0)*, the nonlinear integro-differential equations were solved numerically by using forward finite difference approximation for time derivative, centered finite difference approximation for the position derivative and applying the trapezoidal rule to evaluate the integrals using MATLAB.

2.2.3 HC Reactor Model

The product from the last HDS reactor bed is cracked into lighter and valuable products in the third HC bed in the presence of hydrogen. Sildir et al. [22] developed a reactor model for an industrial hydrocracking unit by applying the continuous lumping approach. The model predictions were in a good agreement with the plant measurements. Here, the same model for the last bed was used. It is assumed that there is no HDS reaction taking place during hydrocracking. Modeling equations are:

$$\frac{\partial c(k,z,t)}{\partial t} = -v\frac{\partial c(k,z,t)}{\partial z} - k_{hc0}e^{\frac{-E_{a,hc}}{R}\left(\frac{1}{T}-\frac{1}{T_0}\right)}c(k,z,t) + \int_{k}^{k_{hc,\max}} p(k,K)K_0 e^{\frac{-E_{a,hc}}{R}\left(\frac{1}{T}-\frac{1}{T_0}\right)}c(K,z,t)D_{hc}(K)dK \quad (2.16)$$

$$\frac{\partial T(z,t)}{\partial t} = -v\frac{\partial T(z,t)}{\partial z} + \frac{\int_0^{k_{hc,\max}} k_{hc0}e^{\frac{-Ea_{hc}}{R}\left(\frac{1}{T}-\frac{1}{T_0}\right)}c(k,z,t)(-\Delta H_{r,hc}(k))D_{hc}(k)dk}{\int_0^{k_{hc,\max}} c(k,z,t)C_p(k)D_{hc}(k)dk} \quad (2.17)$$

where $c(k,z,t)$ is the mass fraction of hydrocarbon species with reactivity k at axial position z at time t. The term on the left side of Eq. 2.16 denotes accumulation of mass. The first term on the right hand side of Eq. 2.16 is the net rate of addition of mass by convection; the second term is the consumption of the species with reactivity *k* due to cracking; and the third term is the generation of the species with reactivity *k* by cracking the heavier species. The yield function $p(k,K)$ represents the formation of the species with reactivity *k* from hydrocracking of heavier species that has reactivity *K*. $D_{hc}(k)$ is the species type distribution function for the cracking species whose mathematical expression is different than the distribution function $D(k)$ given for hydrodesulfurization. $p(k,K)$, $\Delta H_{r,hc}(k)$ and $D_{hc}(k)$ are specified in [22]. In Eq. 2.17, the second term on the right hand side is the addition of heat due to cracking; $C_p(k)$ and $\Delta H_{r,hc}(k)$ are the heat capacity and heat of reaction of species with reactivity *k*, respectively.

The initial distribution *c(k,0,0)* and the HC integro-differential equations are solved by the same numerical methods desribed for hydrodesulfurization. After the product concentration $c(k,z,t)$ is calculated by solving the differential equations, the weight fraction of each product can be determined from:

$$w_{1,2}(z,t) = \int_{k}^{k_2} c(k,z,t) D_{hc}(k) dk \tag{2.18}$$

2.3 Feed Characterization

In order to simulate the first HDS bed, the weight fraction of sulfur in the feed has to be known. In the plant, sulfur concentrations of certain distilled volume fractions of the feed are measured by using ASTM D2622 method in which the total sulfur content of each fraction is measured by a wavelength X-ray Fluorescence Spectrometry. For a particular day of operation, these laboratory measurements are given in Table 2.1.

Table 2.1: Feed sulfur measurements for a particular day.

Feed	S (wt%)
ASTM IBP	0
20 vol%	0.47
50 vol%	0.60
95 vol%	1.04
ASTM FBP (100%)	1.121

By fitting a polynomial using the measurements in Table 2.1, the cumulative sulfur distribution is constructed with respect to TBP as shown in Figure 2.5a. Since the cumulative distribution function is the integral of the density function, the sulfur density function is computed by differentiating the cumulative distribution and plotted in Figure 2.5b. The HDS model uses the weight fraction of sulfur in the feed w_i (see Eq. 2.10). This corresponds to the

sulfur density shown in Figure 2.5b. As a final note, sulfur density which is given as a function of TBP in Figure 2.5b can be expressed in terms of reactivity *k*, by using the mapping between *k* and the normalized TBP θ given by Eq. 2.4.

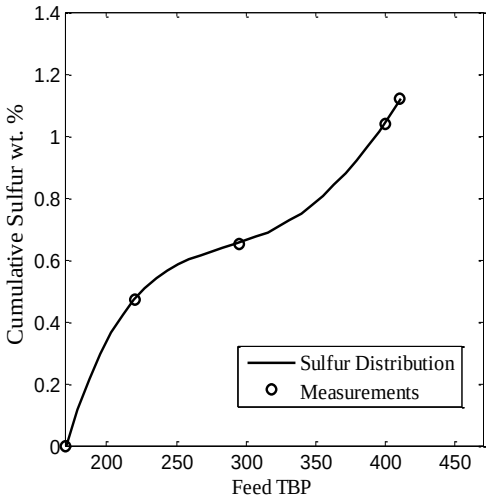

Figure 2.5.a: Cumulative distribution function for sulfur.

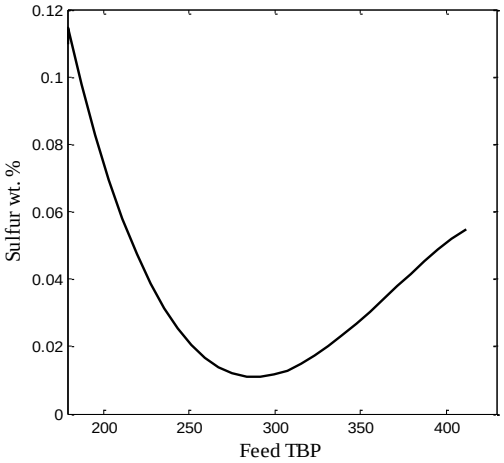

Figure 2.5.b: Sulfur density function

In addition to the feed sulfur distribution, it is necessary to characterize the composition of the hydrocarbons in the petroleum feed as well. True boiling point (TBP) curve is a common way to characterize the composition of crude oil. ASTM D86 method is used in order to generate the TBP curve of a petroleum mixture by distillating certain volume fractions of the mixture using lab scale distillation columns [23]. Using an industry - standard ASTM D86 in the laboratory, distilled volume fractions of the feed are recorded as a function of temperature. For a particular day, these measurements are tabulated in Table 2.2.

Table 2.2: ASTM D86 results for a particular day

	DHP FEED DRUM
API	34.0
S (w%)	1.31
distillation type	**ASTM D86**
ASTM IBP , ˚C	205
5 vol% , ˚C	227
10 vol% , ˚C	247
30 vol% , ˚C	278
50 vol% , ˚C	303
70 vol% , ˚C	328
90 vol% , ˚C	365
95 vol% , ˚C	386
ASTM FBP , ˚C	401

From the volume fractions, the weight fractions can be computed (e.g. using the oil manager of HYSYS) and plotted versus temperature to give the TBP curve. In addition to the feed, Diesel and Naphtha TBP curves are also measured in plant. Using these measurements and blending them in HYSYS Oil Manager, product TBP curve can also be estimated.

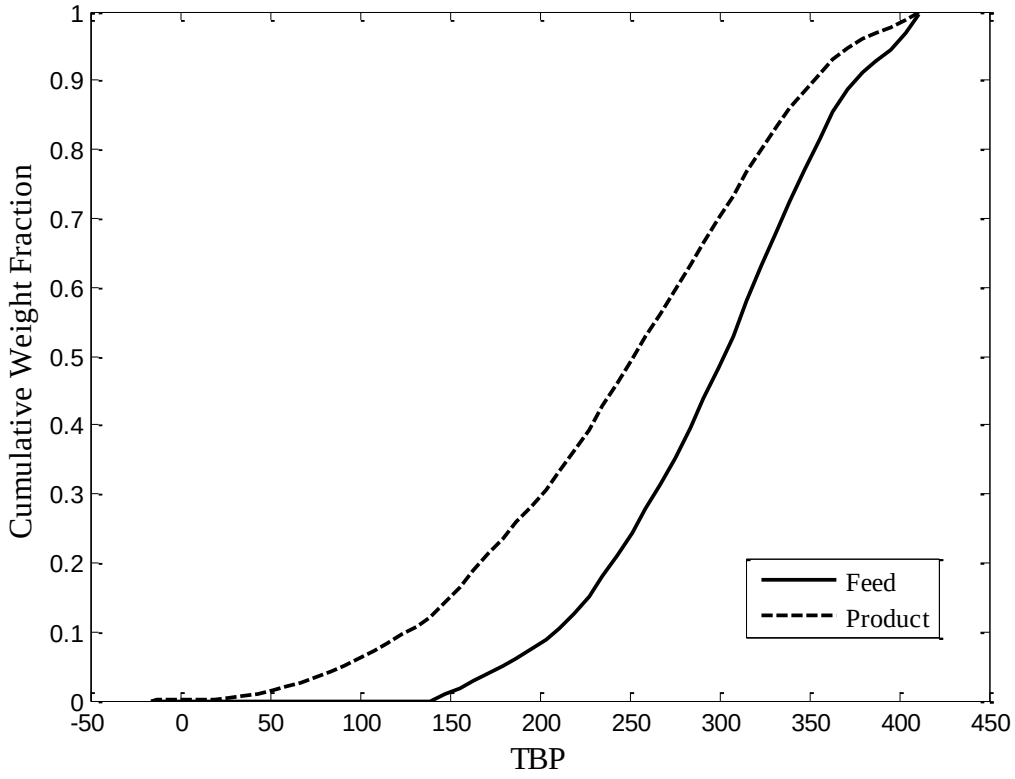

Figure 2.6. TBP Curve of Feed and Product of DHP.

2.4 Results and Discussion

2.4.1 Parameter Estimation

Having developed the structure of the model, parameter estimation methods can be used to determine appropriate values for the parameters so that the model's predictions match the plant data closely. Steady-state parameter estimation is defined as a non-linear weighted least squares problem:

$$\min (X_p - X_m(\phi))^T W (X_p - X_m(\phi)) \tag{2.19}$$

where X_p is the vector of plant measurements; $X_m(\phi)$ is the vector of model predictions which depend on the values of the parameter set ϕ. W is a weighting matrix. Available plant output measurements for the HDS reactors are the temperature differences in each reactor bed and the sulfur content of the product. The plant measurements for the HC unit consist of the temperature difference across the bed and the weight fractions of the diesel and naphta products after fractionation (see Figure 2.6). Once the TBP curve of the HC reactor effluent is predicted by the HC model, the weight fractions of the end products diesel and naphta can be easily calculated (see Results) and compared with the measured values in the plant. Adjustable parameters for the hydrodesulfurization and the hydrocracker reactors are given in Table 2.3 and Table 2.4 [22], respectively.

Table 2.3. HDS Parameters

Parameter	Description
$k_{\min 1}$	Minimum reactivity of sulfur species in Bed 1
$k_{\min 2}$	Maximum reactivity of sulfur species in Bed 2
β	The parameter that relates HDS reactivity to the normalized boiling point
$k_{\max 1}$	Maximum reactivity of sulfur species in Bed 2
$k_{\max 2}$	Maximum reactivity of sulfur species in Bed 2
E_{a1}	Activation energy of Bed 1
E_{a2}	Activation energy of Bed 2
ΔH_1	Heat of Reaction in Bed 1
ΔH_2	Heat of Reaction in Bed 2

Table 1.4. HC Parameters.

Parameter	Description
$k_{hc,\max}$	Maximum reactivity of hydrocarbon species
α	The parameter that relates cracking reactivity to normalized boiling point
α_0	The parameter in the yield function
α_1	The parameter in the yield function
$E_{a,hc}$	Activation energy for the hydrocracking reactions
c	Parameter for the heat of cracking reaction
d	Parameter for the heat of cracking reaction

For such complex systems and high number of parameters, some of the parameters may be correlated, unidentifiable or redundant, meaning that they have poor (large) confidence intervals. In order to have reliable estimates, the most sensitive and reliable set of parameters have to be tuned and the other parameters should be fixed at some nominal values. Fisher Information matrix is used for this purpose [22], [24], [25]. First, parameter estimation is done without fixing any of the parameters and an initial parameter set is obtained. Next, following the algorithm given in Schittkowski [25], the number of parameters is reduced by specifying a minimum threshold for the eigenvalues of Fisher information matrix. Parameter selection is finalized with the four parameters listed in Table 2.5 since adding more adjustable parameters increased the 95% confidence limits. These four parameters were tuned as process conditions changed from day to day. The rest of the parameters were fixed at the nominal values taken from the initial parameter set, which gave consistent and reasonable prediction errors. These nominal values are listed with their literature ranges in Table 2.6. When the fixed parameters are compared with the literature values, it is seen that all the estimated parameter are consistent with the literature ranges.

Table 2.5. Identifiable Parameters for DHP Unit

Parameter	**Nominal Value**	**95 % Confidence Interval**
$k_{\min 1}$	0.298	0.094
$k_{\min 2}$	0.254	0.054
ΔH_1	-7400	0.056
$k_{hc,\max}$	0.106	0.012

Table 2.6. Fixed Parameters.

Parameter	Nominal Value	Literature Values
k_{max1}	1.5	7.5 [8]
k_{max2}	1.5	7.5 [8]
ΔH_2	-41970	-57000 [26], -13000 to -68000 [27]
Ea_1	47700	79800 to 244740 [28]
Ea_2	99800	52000 to 272000 [27]
Ea_{hc}	150000	137000 to 70000 [29]
c	-0.0111	-
d	-111	-136.7 [22]
α	0.5065	1.35 [30], 0.72 [31], 0.35 [8]
a_0	0.9629	1.5 [8], 3.08 [31]
a_1	20.39	22 [8], 26 [31]

2.4.2 Steady State Results

The following variables are measured in the plant: amount of removed sulfur, the temperature differences in each reactor bed, the TBP curves of the the products naphta and diesel (including the T95 point of Diesel) and the total amounts of naphta and diesel products. In the plant it is not possible to perform a distillation assay on the reactor output before fractionation due to safety restrictions. Instead ASTM D86 distillation is performed on naphta and diesel products obtained after fractionation. These individual assays are blended by the HYSYS oil manager to yield the total product's TBP curve. The results are shown in Figure 2.7. As seen in Fig. 2.7 TBP curves of naphta and diesel overlap in the boiling range $\theta = 0.30$ - 0.47 indicating that the separation is not 100%. This has to be taken into account when calculating the individual weight fractions of or amounts of naphta and diesel. The temperature cut point (TCP) concept was used to calculate the individual amounts of naphta and diesel products [32]. For two "adjacent" products whose TBP curves overlap, the temperature cut point is defined by

$$TCP = \frac{IBP(h) + FBP(l)}{2} \tag{2.20}$$

where *IBP(h)* is the initial boiling point of the heavy product diesel, and *FBP(l)* is the final boiling point of the light product naphta. From Eq. 2.20 the calculated cut point temperature is 0.367. The intersection of *TCP* with the product curve defines the weight fraction of naphtha which is equal to 0.12. Assuming that the content of off-gas and residue in the distillation unit is negligible, the weight fraction of diesel can be estimated by subtracting the weight fraction of naphtha from 1 to get 0.88. This assumption is reasonable since off-gas and residue contents are not measured in the plant due to their negligible amounts relative to the main products naphtha and diesel. Analysis of fractionation data from different days has shown that the temperature cut point is kept constant from day to day operation. Therefore the value 0.367 is used in the predictions. Figure 2.7 compares the model predicted TBP curves of the product with plant data. Product-Model is the TBP curve of the product leaving the last HC bed as predicted by the model. Product-Plant refers to the TBP curve which is constructed by blending the naphta and diesel TBP curves obtained from plant data. The match is very good.

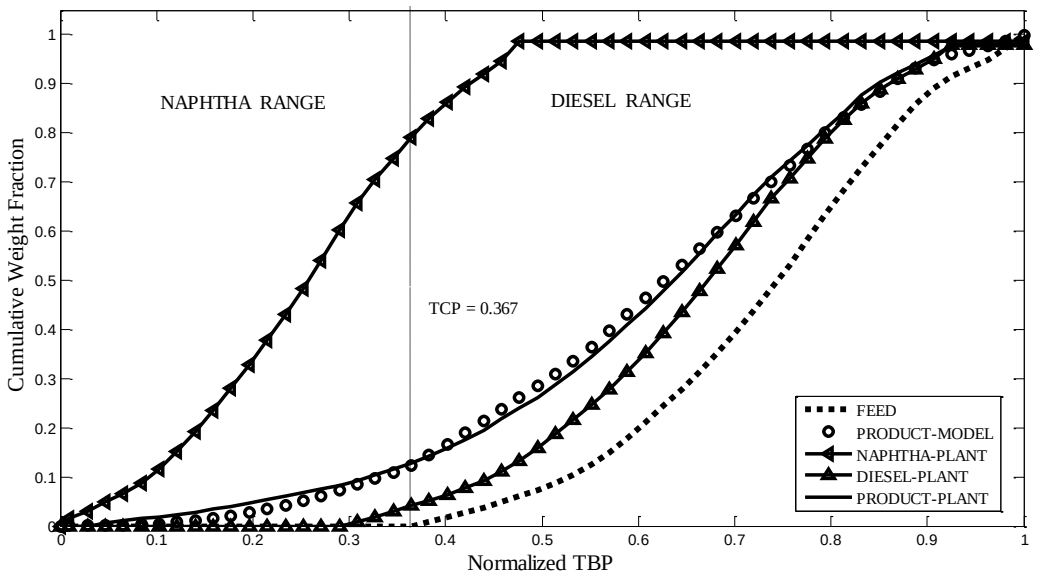

Figure 2.7. TBP curves for the particular day.

The model is trained using steady-state plant data for three different days, and is simulated for four different days to check the prediction performance. The results are given in Fig. 2.8. The closer the data is to y-x line the smaller the training or the prediction error is. For better quantification, AAD (Average Absolute Deviation) and RMSE (Root Mean Square Error) values are also given in Table 2.7. The errors are less than 5% individually and 2% in average and they can be considered within process noise and measurement error limits.

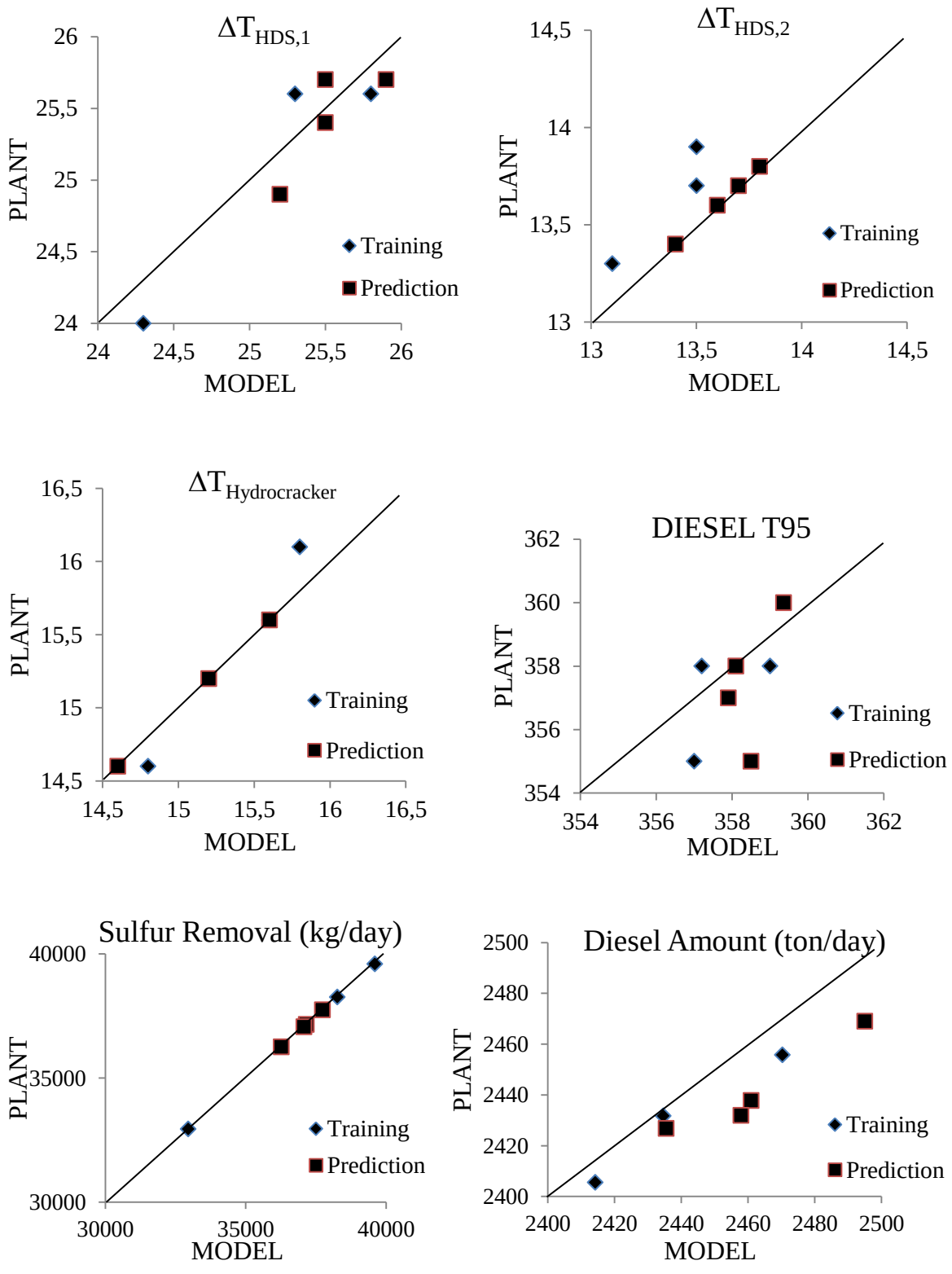

Figure 2.8. Training-Prediction Results.

For a particular day, the sulfur removal in the hydrodesulfurization beds is given in Fig. 2.9.

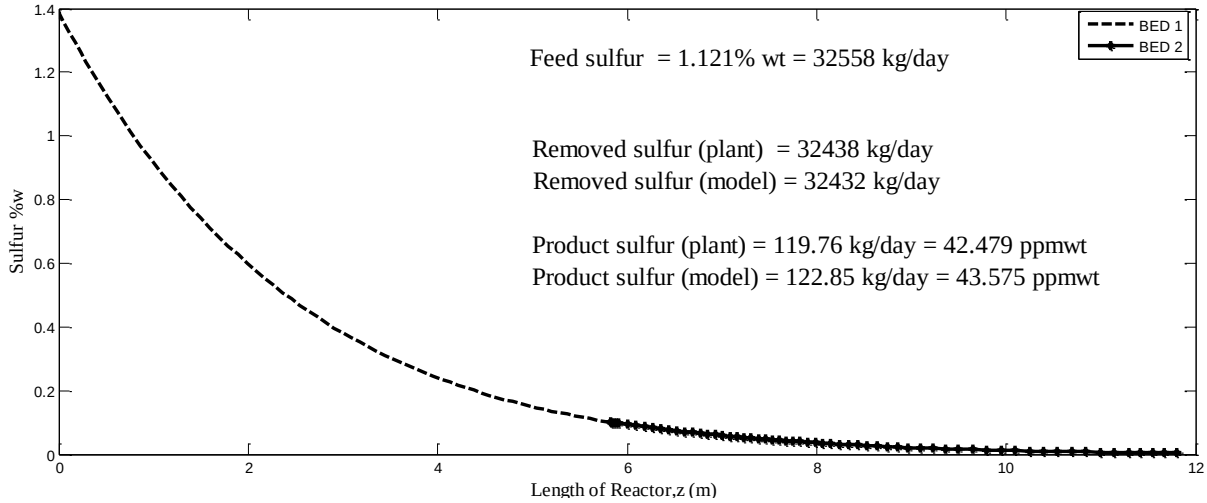

Figure 2.9. Sulfur removal along the hydrodesulfurization beds.

Sulfur removal is predicted very well as shown by the numbers in Figure 2.8 and 2.9. The lower-boiling point sulfur compounds have higher reactivities and most of them are removed in the first bed while the hard-to-remove higher boiling point sulfur compounds are removed in the second bed. This is confirmed by the sulfur distributions shown in Figure 2.10. Note that sulfur amounts in bed 1 and bed 2 are small compared to the feed; therefore, they are scaled to be able to see the changes in the sulfur distribution.

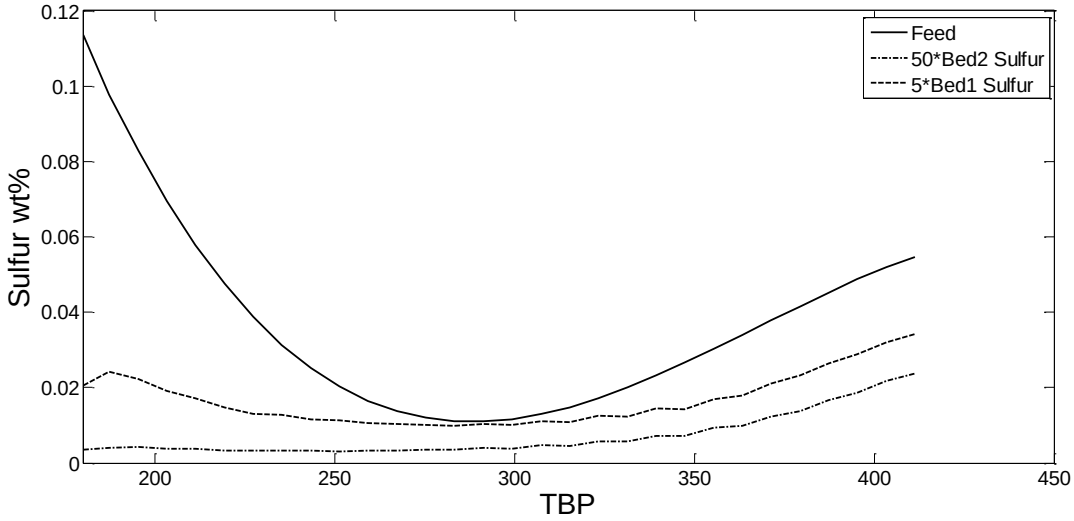

Figure 2.10. Sulfur density in hydrodesulfurization.

2.4.3 Dynamic Results

In the plant the reactor bed temperatures are measured and controlled to achieve the desired amount of sulfur removal and the diesel product. Therefore the bed temperatures are the key variables and the model should be able to correctly predict their dynamic responses. The dynamic performance of the model was evaluated under transient conditions by using step testing data obtained from the plant. This data was generated by changing the inlet temperatures and measuring the exit temperatures of the beds. In the plant, the inlet temperatures of the reactor beds are adjusted by the PID controllers which manipulate the hydrogen quench flows between the beds (see Figure 2.1). Therefore, the dynamic response of the inlet temperatures to a set-point change was first approximated by identifying first-order transfer functions from plant measurements (see the inlet temperatures in Figures 2.11-2.14). Next this model is simulated together with the first-principles reactor model. Results are shown in Figures 2.11-2.14. The model is able to capture the dynamics of the plant. Please note that all the results are scaled by a constant value due to the proprietary reasons.

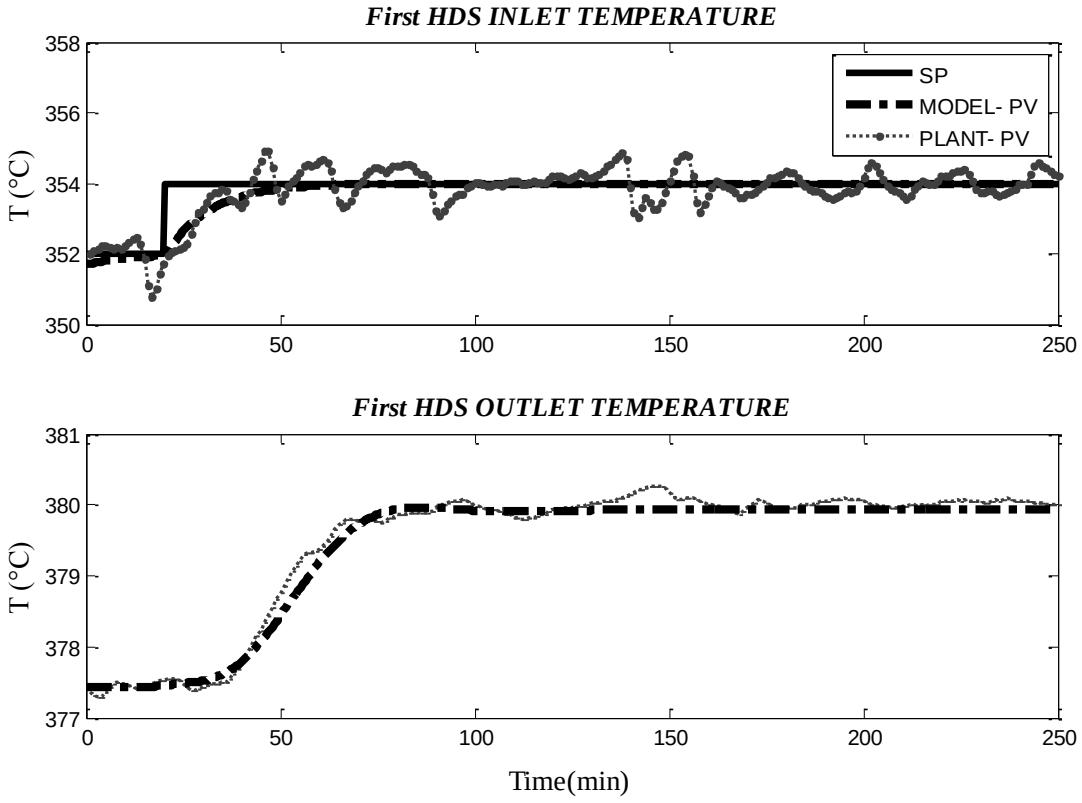

Figure 2.11. Dynamic response of the first HDS bed to a step increase in inlet temperature.

(SP: set point. PV: process value)

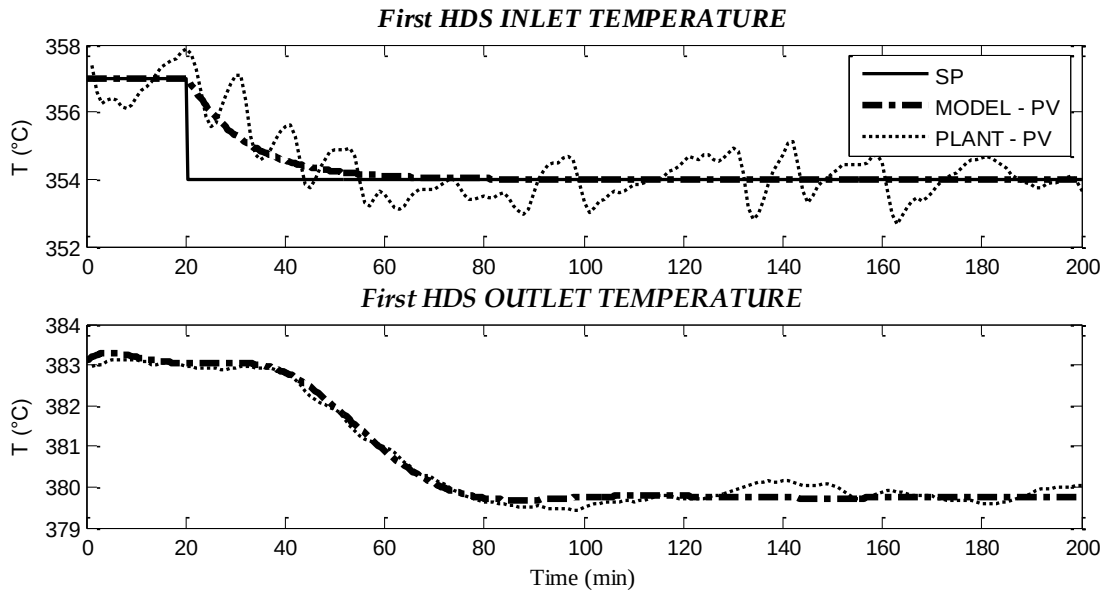

Figure 2.12. Dynamic response of the first HDS bed to a step decrease in inlet temperature.

(SP: set point. PV: process value)

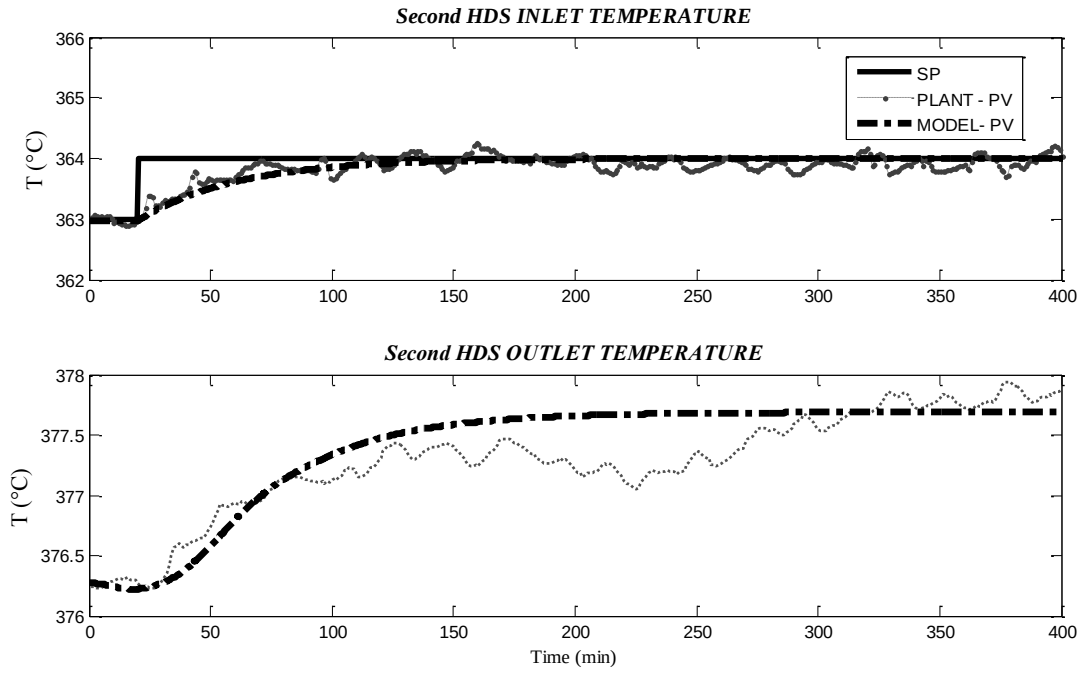

Figure 2.13. Dynamic response of the second HDS bed. (SP: set point. PV: process value)

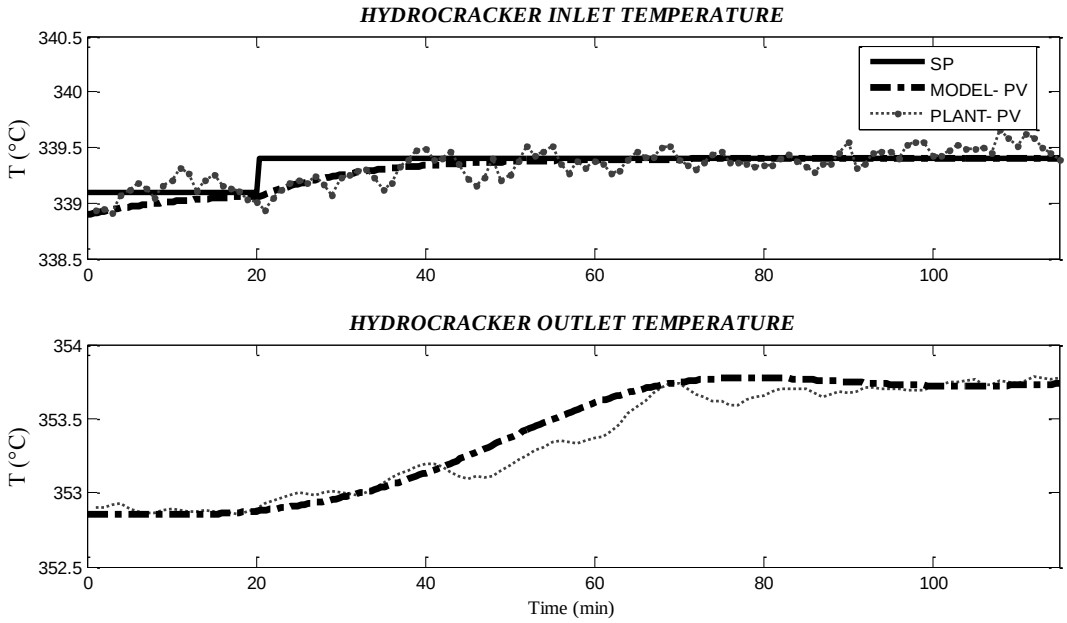

Figure 2.14. Dynamic response of the HC bed. (SP: set point. PV: process value)

It is well known that exothermic fixed bed reactors can exhibit inverse response or wrong-way behavior [33]. As seen in Figure 2.15, the model shows an inverse response (albeit very small) in the outlet temperature response of the second HDS bed. When the inlet bed temperature decreases, the exit temperature initially increases slightly followed by a decrease to its new steady-state value. When the inlet temperature decreases, there is more less conversion at the reactor inlet. The increased concentration travels to the bed exit faster than the temperature and results in a temporary increase in the reaction rate. Thus the temperature initially increases at the end of the bed. This effect is followed by the slower propagation of the temperature decrease which eventually decreases the conversion and the temperature at the outlet; thereby, resulting in the inverse response. Figure 2.16 shows a similar inverse response for the first HDS bed, this time occuring for a temperature increase in the inlet temperature. It is good that the model is able to predict a known phenomeon. However, this effect has been found to be very small and obscured in the plant's responses. This is due to the fact that only small temperature set-point changes are allowed in the plant and there is measurement noise.

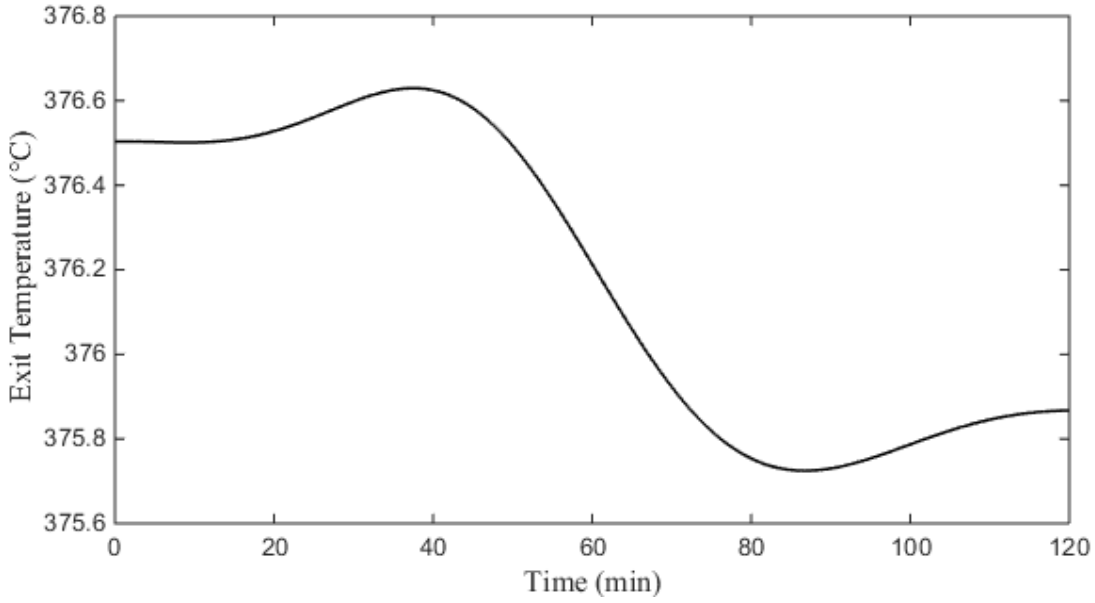

Figure 2.15. Wrong-way behavior for the second HDS bed. Response to a step decrease in the inlet temperature.

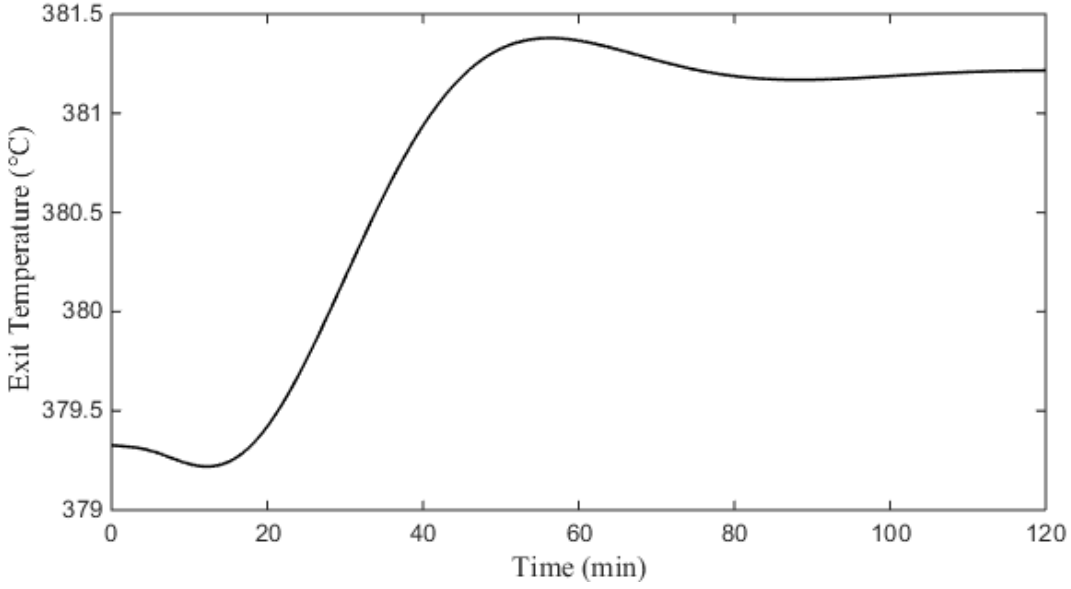

Figure 2.16. Wrong-way behavior for the first HDS bed. Response to a step increase in the inlet temperature.

Finally, the dynamic model is simulated with a heavier feed. The TBP curve and sulfur distribution of the heavier feed are given in Fig. 2.17 and Fig. 2.18, respectively. Simulation results are given in Fig. 2.19 and Fig. 2.20.

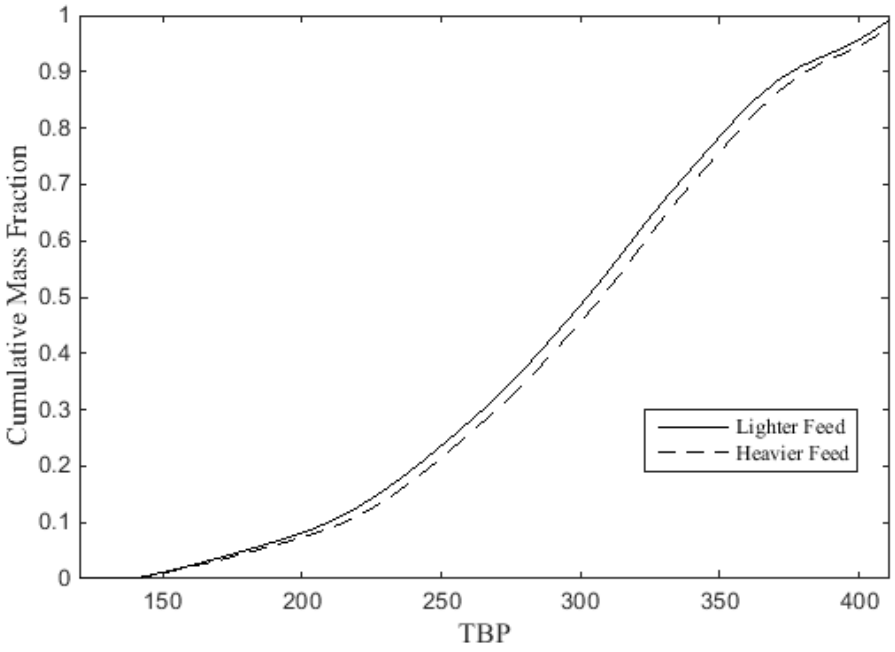

Figure 2.17. TBP curve of the two feeds.

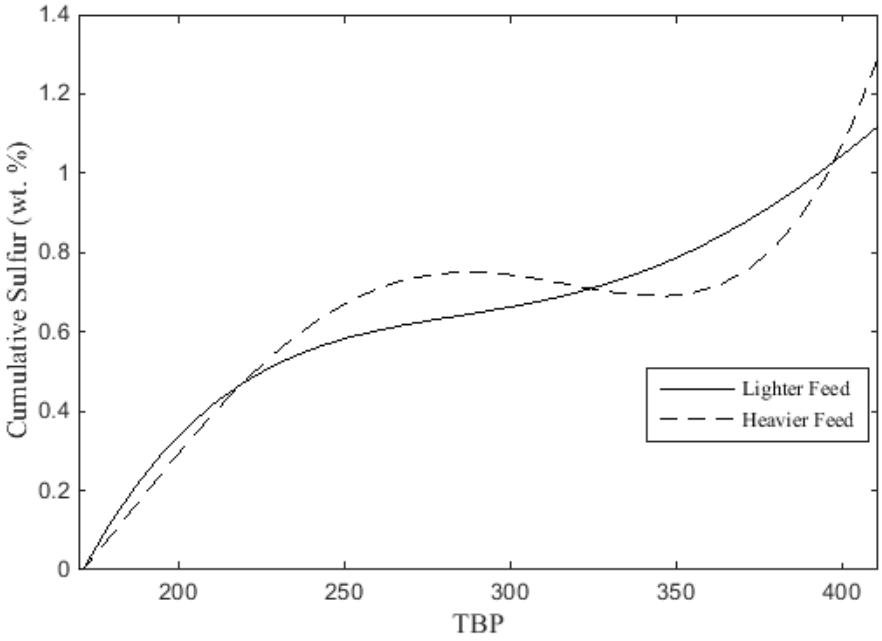

Figure 2.18. Sulfur distribution of the two feeds.

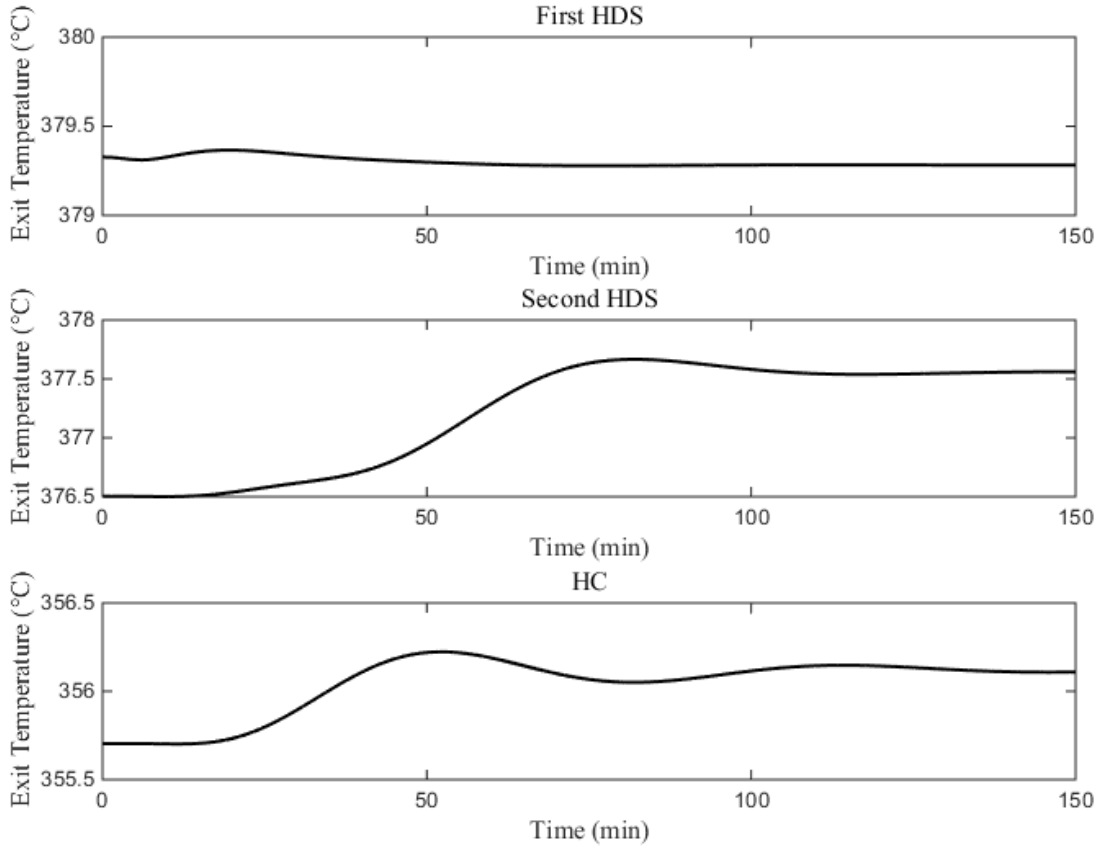

Figure 2.19. Temperature response of the reactors for the heavier feed.

Fig. 2.19 shows that the change in the exit temperature of the first HDS reactor is negligible. The amount of the lower boiling sulfur compounds determines the rate of reaction in the first bed. Since this amount is almost the same for both feeds and the heat of reaction in the first bed is significantly smaller than the second bed, the overall reaction rate and the total sulfur consumption does not change in any significant way. Thus, the change in the exit temperature of the first bed is negligible. However, when the feed gets heavier, the amount of the higher boiling sulfur compounds fed to the second reactor increases. As a result, the total sulfur consumption increases in the second bed. Since the reaction in the second bed is highly exothermic, the temperature in the second bed increases as given in Fig. 2.19. Moreover, as the feed gets heavier, cracking reactivity increases in the hydrocracker resulting in an increase in the exit temperature of the hydrocracker as shown in Fig.2.19. Diesel T95 boiling point increases with the heavier feed when all other process conditions are kept the same.

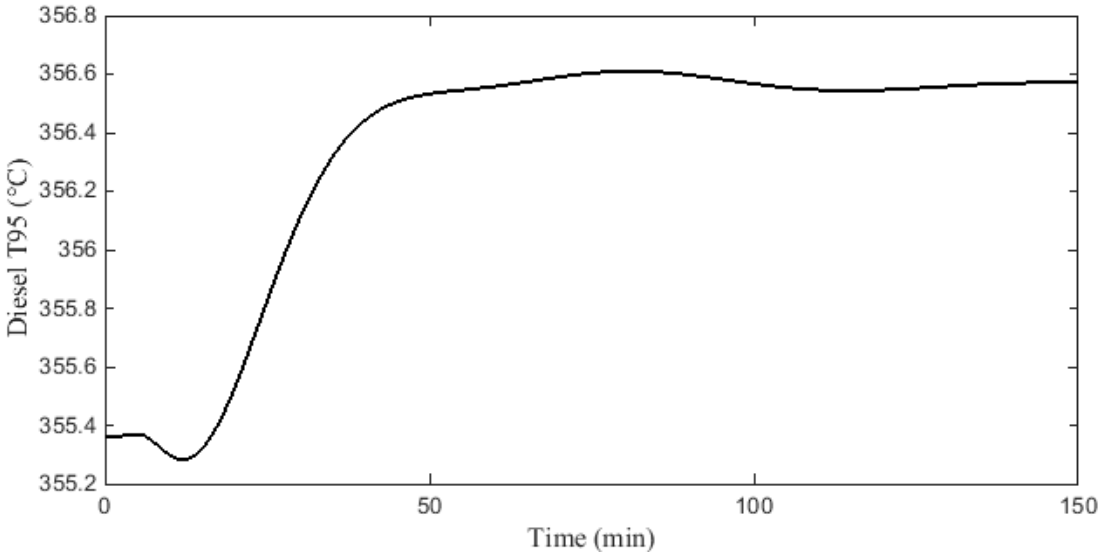

Figure 2.20. Dynamic Diesel T95 response for the heavier feed.

Chapter 3

PLANT-WIDE OPTIMIZATION AND CONTROL OF THE INDUSTRIAL DIESEL HYDROPROCESSING PLANT

3.1 Introduction

Combustion of sulfur compounds in diesel engines emits sulfur oxides into the atmosphere and causes health and environmental problems. Diesel hydro-desulfurization is an important refinery process which removes the undesired sulfur compounds from the oil feedstock. In order to comply with the new emission standards for better air quality, there is an increasing demand for the production of ultra-low sulfur diesel (ULSD) fuel (<10 ppm). In order to meet this low sulfur demand, refineries are now evaluating alternative revamping and control strategies to improve the operation of their hydro-processing plants [2].

The industrial diesel hydro-processing (DHP) plant which is the subject of this study consists of two catalytic hydro-desulfurization (HDS) reactor beds and one hydro-cracking (HC) reactor bed in series as shown in Fig. 3.1. The plant is designed to process 4500 cubic meters per day of diesel feedstock. The feedstock is obtained by blending four streams: HD (straight run heavy diesel), LD (straight run light diesel), LVGO (light vacuum gas oil) and an imported diesel. HD and LD streams are obtained from a crude distillation unit, and LVGO stream is derived from a vacuum distillation unit. These streams are blended in order to obtain a desired T95 value (the temperature at which 95% of the distillate is collected e.g. by ASTM D86 distillation) for the reactor charge. The blended feed is mixed with the recycle hydrogen gas before it enters the furnace where it is heated to the required reactor inlet temperature. In the first two HDS beds, the organic sulfur impurities are removed. Hydrocracking (HC) occurs in the last bed where heavier hydrocarbons are cracked to lower molecular weight petroleum fractions. Inter-stage cooling by quench hydrogen is used in both reactors to control the bed temperatures. Reactor effluent is next separated into useful end products such as naphtha and diesel. In our earlier work, we developed dynamic, non-isothermal, pseudo-

homogeneous plug flow models for the HDS [34] and the HC [22] reactors. These models are trained using industrial data and validated under both steady and dynamic conditions.

The DHP plant operates with various feed-stocks. Also, changing market conditions have significant effects on the diesel product specifications. In the presence of such a dynamic environment, the DHP plant has to run in the most profitable and safe way and satisfy the requirement that the sulfur content of the diesel product meets its specification (in this case below 10 ppm). In this study, we propose a hierarchical, cascaded model predictive control structure for the industrial DHP plant. For the reactors we use the models we have developed earlier. For the feed blending and the fractionation units, we develop new empirical models to predict certain important feed and product properties for optimization and control purposes. These models are briefly explained next to help understand the subsequent real-time optimization and control study which constitutes the focus of this paper.

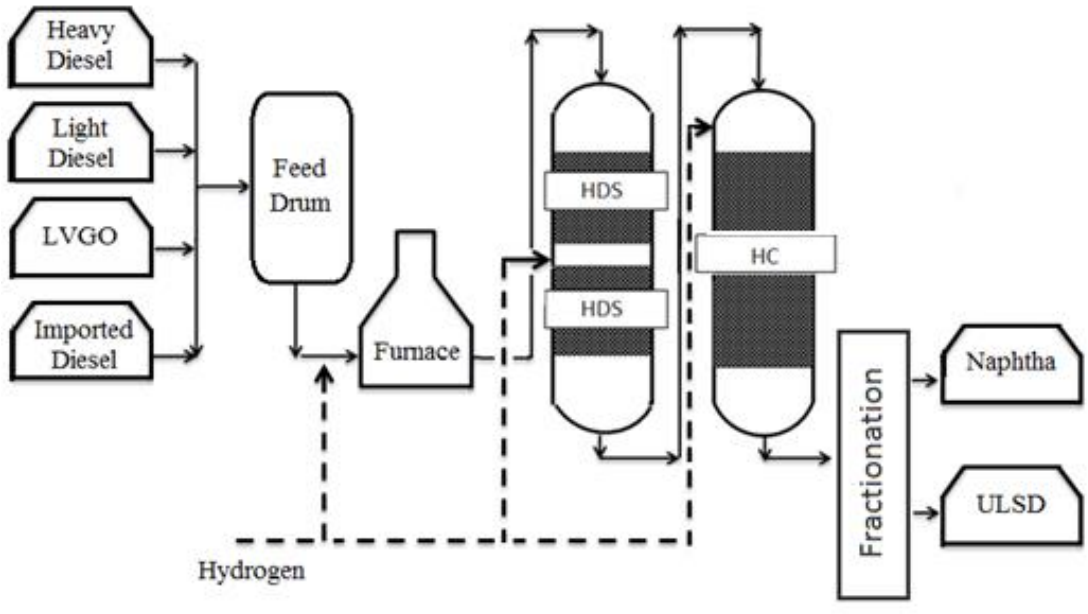

Figure 3.1: Simplified DHP plant flowsheet.

3.2 The Blending Model

The kinetics of hydro-desulfurization is complex since the diesel feedstock contains a variety of organic sulfur compounds with different reactivities. We developed a non-isothermal, plug-flow model using the continuous lumping approach which treats the reaction medium as a continuum of species whose reactivities depend on the true boiling point of the mixture [34]. The reactions are modeled as pseudo homogeneous first order reactions.

The effluent of the second HDS reactor is sent to the hydrocracking reactor where the lighter and valuable products are obtained. Sildir et al. [22] presented a hydrocracker model based on continuous lumping method. This model was adapted to the plant. The hydrocracking model is based on non-isothermal, plug flow reactor model and the reactions are assumed to exhibit first order behavior. Both models are trained using industrial data and validated under steady and transient conditions. The prediction results were good [34].

In the blending subsystem the heavy diesel (HD) and the light diesel (LD) from the upstream atmospheric column, LVGO from the upstream vacuum distillation column and the imported tank diesel are mixed to form the feed to the downstream DHP reactors (see Fig.3.2). In order to simulate the DHP model, the weight fraction of sulfur in the feed has to be known as a function of distilled volume fractions of the feed. In addition, we need to characterize the composition of the hydrocarbons in the petroleum feed as well. D86 curve is a common way to characterize the composition of crude oil. Using an industry - standard ASTM method in the laboratory, distilled volume fractions of the feed are recorded as a function of temperature. The plot of temperature versus the distilled volume fractions gives the D86 curve.

While both the sulfur content and the D86 curve of the feed are measured in the plant, we need to be able to predict them on-line for optimization and control purposes. For this reason, we developed empirical models to estimate the sulfur content and the D86 curve of the DHP feed from other available measurements.

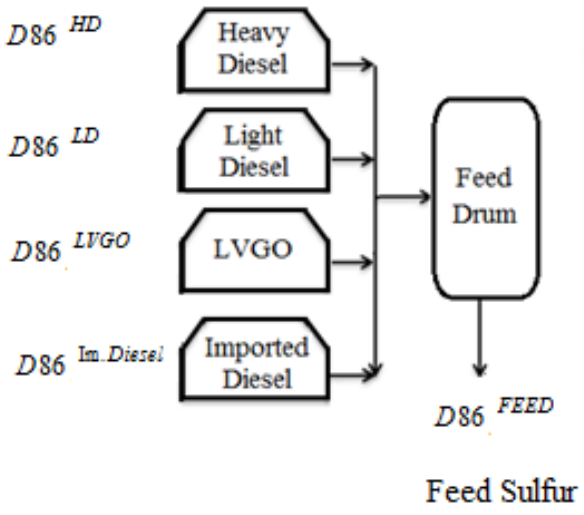

Figure 3.2. DHP Blending Subsystem.

3.2.1 Estimation of the D86 Curve of the Feed

The individual D86 of the four blended streams and of the feed drum are measured on a continuous basis every eight hours. Using these measurements, the Feed D86 curve is constructed from the following least-squares model:

$$D86_i = (D86_i^{HD})(x^{HD})(a_i) + (D86_i^{LD})(x^{LD})(b_i) + (D86_i^{LVGO})(x^{LVGO})(c_i) + (D86_i^{Im.Disel})(x^{Im.Diesel})(d_i) \quad (3.1)$$

where *i*' s are the measured distillation points (i.e. 0, 5,10 ,30, 50,70, 90, 95,100 vol %); *x*' s are the mass fractions of the blended raw materials; a_i, b_i, c_i, d_i are the parameters to be estimated. A set of 110 shifts of industrial data is used for the training and validation of the blending model. Half of the data is used for training and the other half is used for prediction. The estimated parameters along with the training and validation errors are given in Table 3.1.

Table 3.1. The Blending Model Results

Parameters	**0 %**	**5%**	**10%**	**30%**	**50%**	**70%**	**90%**	**95%**	**100%**
a_i	0.35	0.53	0.76	0.95	0.9	0.97	1.1	1.12	1.08
b_i	1.5	1.55	1.3	1.1	1.2	1.09	0.97	0.97	1.00
c_i	0.68	0.607	0.74	0.79	0.88	0.975	1.0	1.09	1.09
d_i	0.93	0.91	0.95	0.99	0.98	1.0	1.0	1.00	1.00
Training errors (^oC)									
STD	3.1	4.0	2.36	2.1	2.55	2.8	2.7	2.8	2.6
AAD	2.5	3.3	1.8	1.5	1.84	2.0	2.1	2.2	1.96
RMSE	3.0	3.8	2.2	1.9	2.43	2.6	2.6	2.66	2.6
Validation errors (^oC)									
STD	3.8	4.3	2.7	2.14	2.23	2.12	2.24	2.5	3.1
AAD	3.1	3.09	2.8	3.5	2.74	1.88	1.68	1.94	2.45
RMSE	3.7	3.94	3.3	3.8	2.9	2.16	2.23	2.46	2.96

It is seen that the average absolute deviations (AADs) and root mean square errors (RMSEs) are all less than 3.9 ^{0}C. This error value is acceptable for the process. Moreover, Fig. 3.3 shows that the blending model is able to capture the trend of the D86 measurements.

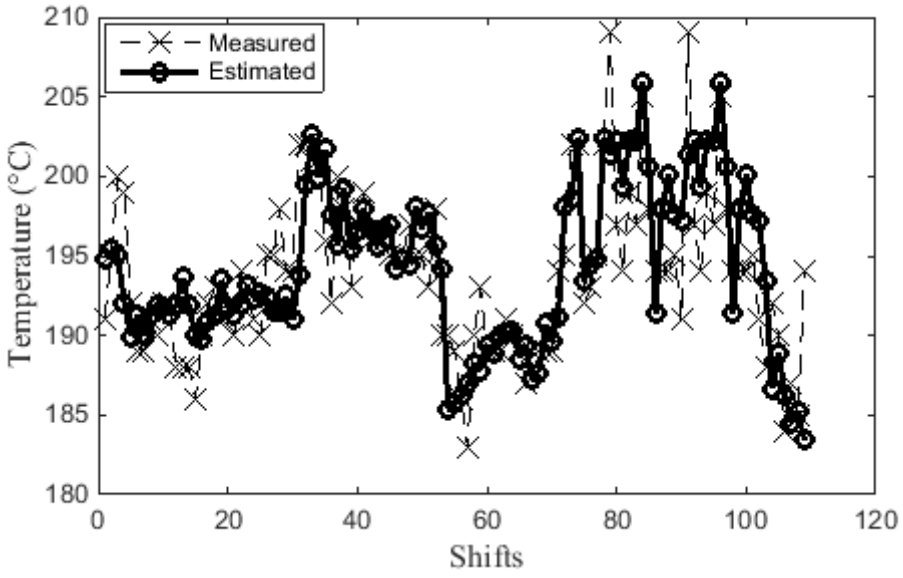

Figure 3.3.a 0 vol % (initial boiling point) D86 estimation.

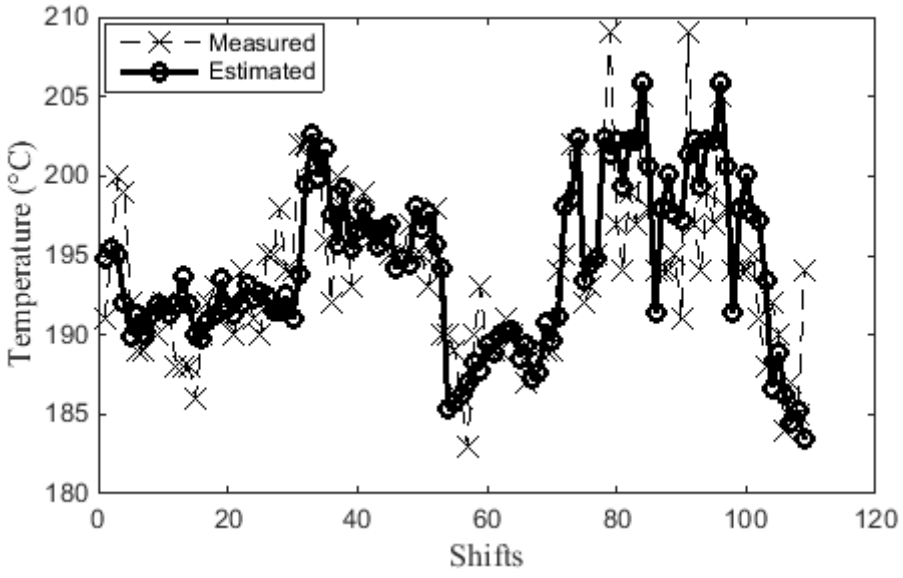

Figure 3.3.b 5 vol % D86 estimation.

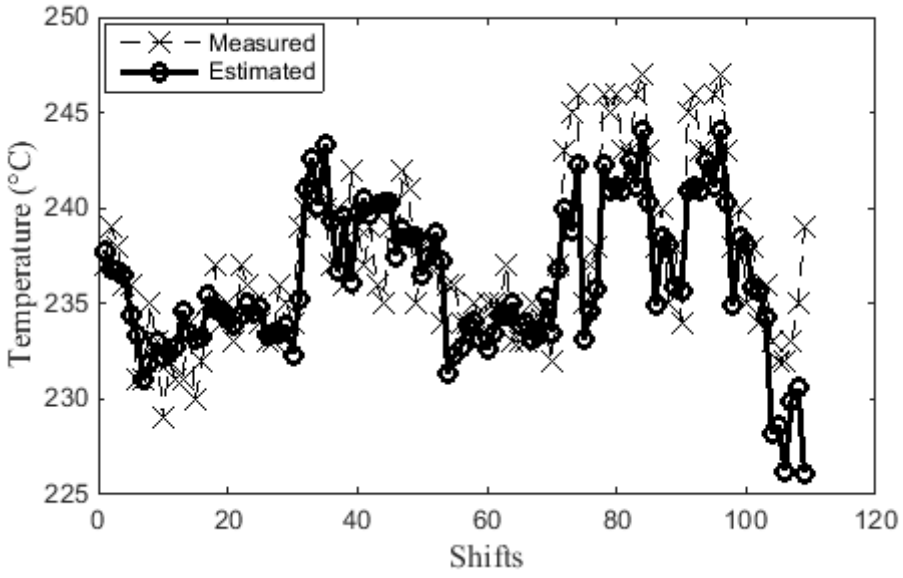

Figure 3.3.c 10 vol % D86 estimation.

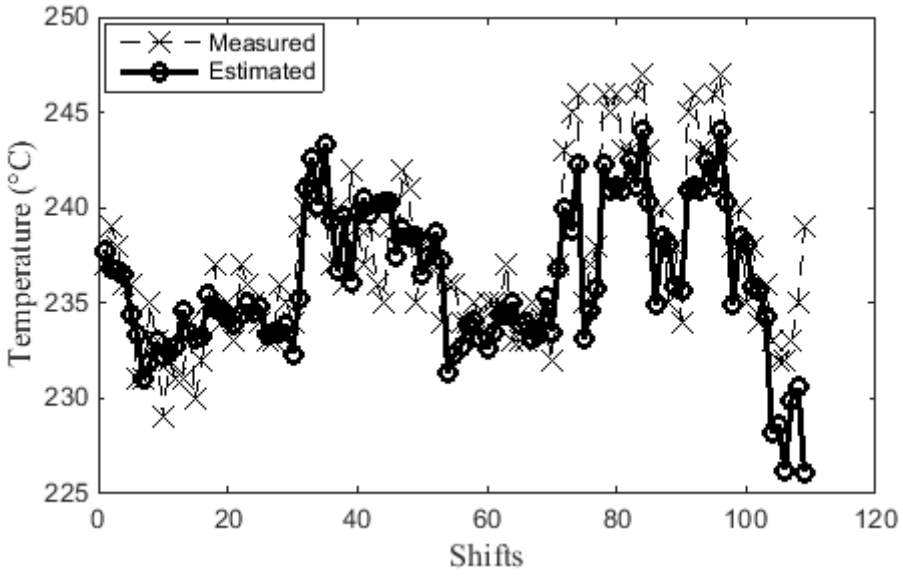

Figure 3.3.d 30 vol % D86 estimation.

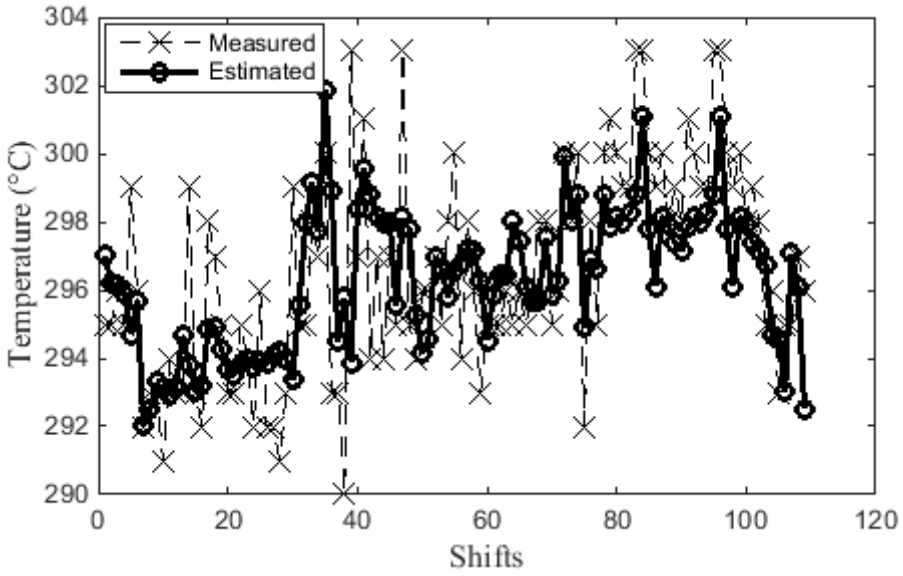

Figure 3.3.e 50 vol % D86 estimation.

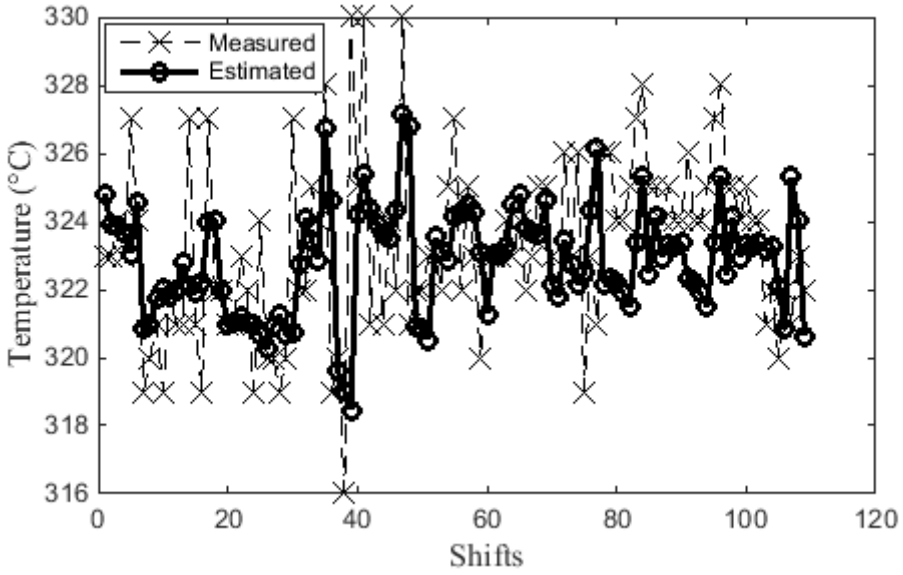

Figure 3.3.f 70 vol % D86 estimation.

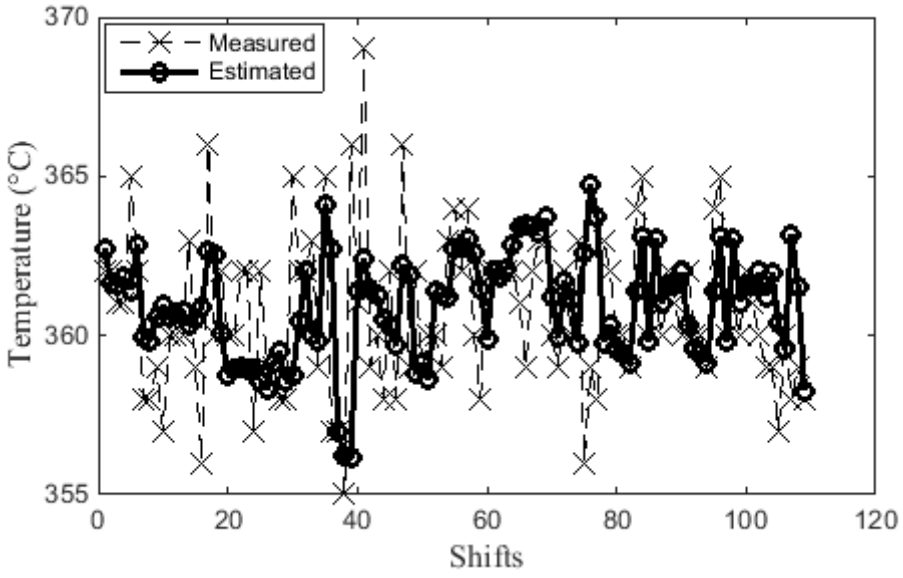

Figure 3.3.g 90 vol % D86 estimation.

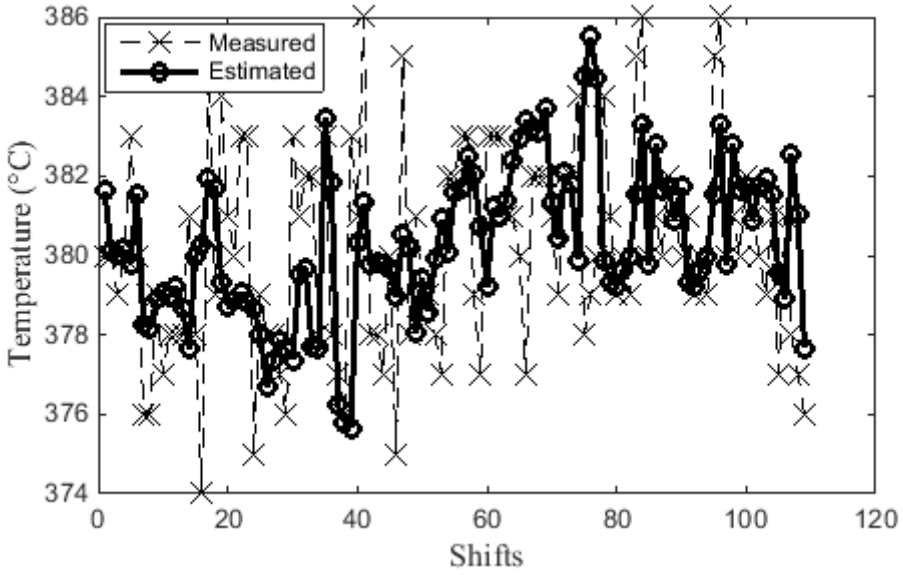

Figure 3.3.h 95 vol % D86 estimation.

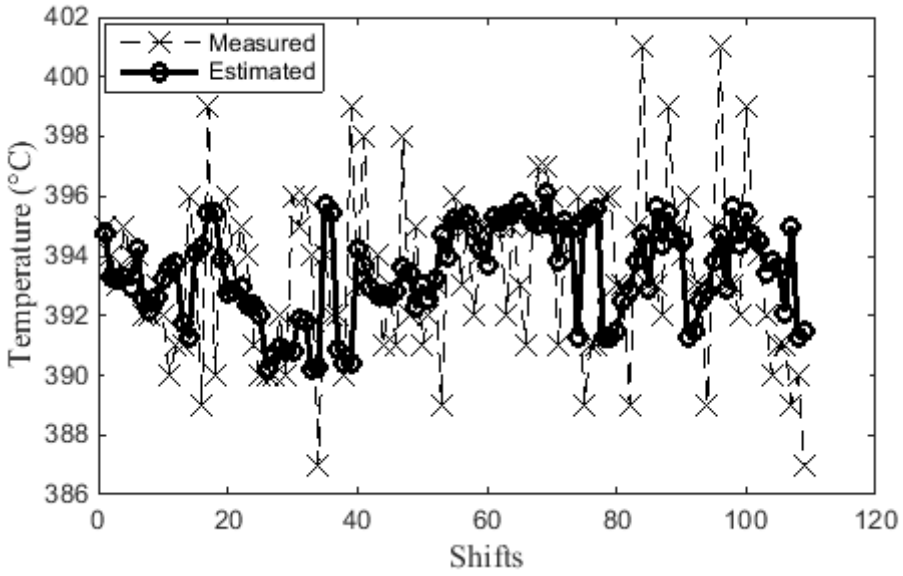

Figure 3.3.i 100 vol % D86 (final boiling point) estimation.

D86 curve estimated for a particular day is given in Fig. 3.4.

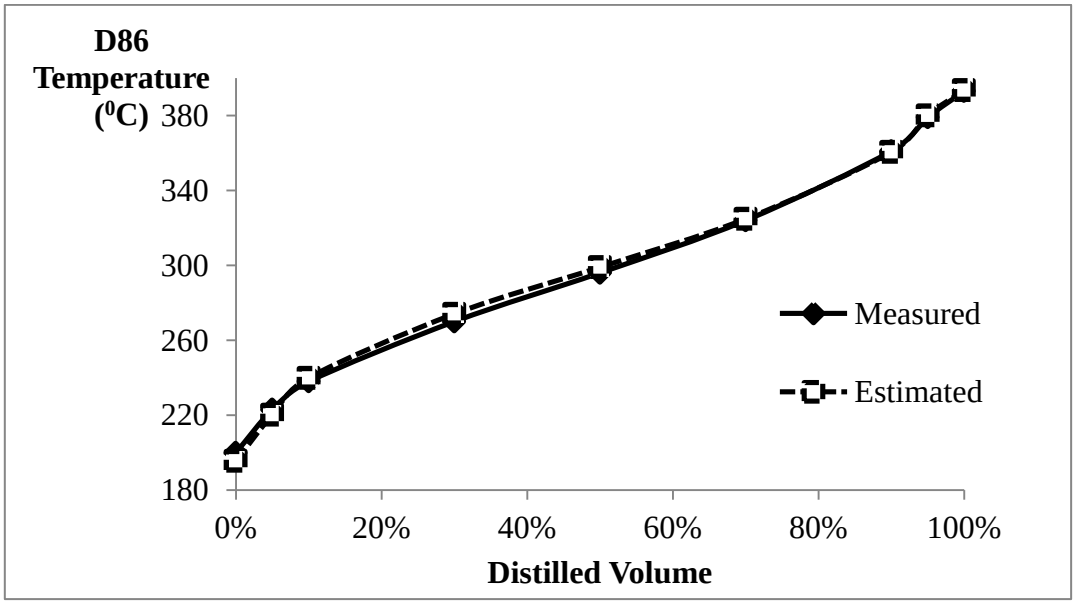

Figure 3.4. D86 curve estimation for a particular day.

3.2.2 Estimation of the Feed Sulfur Content

The reactor model requires the distribution of sulfur in the feed as a function of distilled volume fractions of the feed. However, only the total sulfur concentration (i.e. 100 vol %) is measured in the plant on a continuous basis. Therefore, the model assumes that the total sulfur content S_f (wt%) is uniformly distributed over the boiling range of the feed. The total sulfur content of the reactor feed is estimated from the feed D86 measurements $D86_i^{FEED}$ and the total mass flow-rate $F_f\,(kg/h)$ using linear least squares:

$$S_f = A \times F_f + \sum_i B_i \times D86_i^{FEED} \tag{3.2}$$

where A and B_i*'s* are the parameters to be determined. 30 shifts of measurements were used for training and 10 shifts were used for prediction. The result is given in Figure 3.5 and the errors are listed in Table 3.2. The model can capture the real trend and the match is good

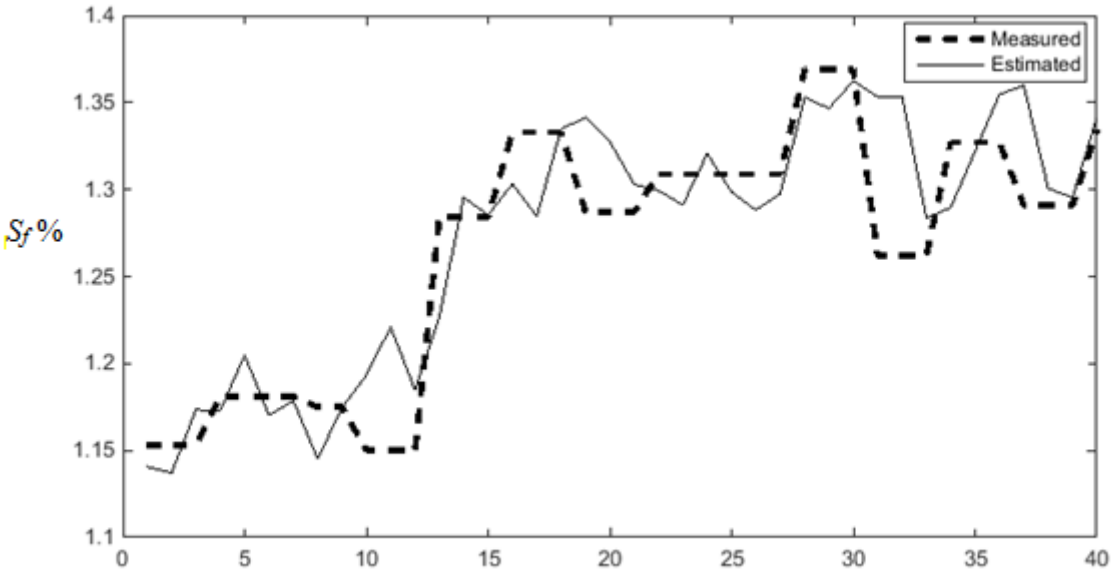

Figure 3.5: Feed Sulfur content estimated by the empirical model.

Table 3.2. Feed Sulfur content estimation results.

Feed Sulfur (S_f%)	
Training error (S_f%)	
STD	0.0288
AAD	0.022
RMSE	0.0262
Validation error (S_f%)	
STD	0.0427
AAD	0.0364
RMSE	0.0402

For both empirical models, the predictions did not improve when different nonlinear models were tried. Therefore, the above linear models were used by the optimization and control algorithms. In addition Kalman Filtering was used to update the model outputs for both Feed D86 curve and Feed sulfur when their measurements were available:

$$\hat{x}(k|k) = \hat{x}(k|k-1) + K(x(k) - \hat{x}(k|k-1) \tag{3.3}$$

where $\hat{x}(k|k)$ is the current estimate of the output after measurement update, $\hat{x}(k|k-1)$ is the output predicted by the model before it is corrected by the measurement. Sampling time k is eight hours since measurements are available once a shift. $x(k)$ is the current measurement and K is the filter gain.

First order tank dynamics was added to the empirical blending model to include the mixing dynamics of the blending tank as in Figure 3.6.

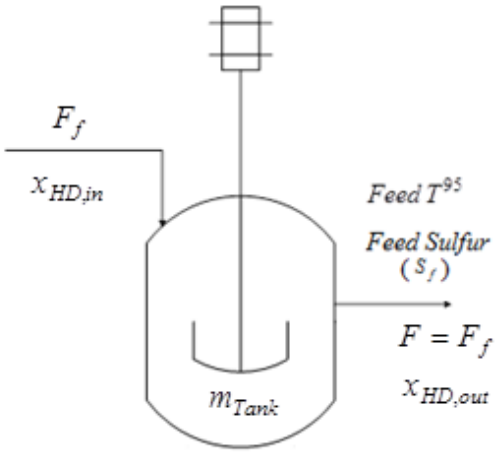

Figure 3.6. DHP Feed Drum.

The derivation of the mass flow rate equations in the tank is as follows.

Suppose component balance on heavy diesel is written, assuming constant volume, perfect mixing in the tank and the total flow rates into and out of the tank are constant:

$$F_f\,(x_{HD,in} - x_{HD,out}) = \frac{d(m_{Tank}\,x_{HD,out})}{dt} \tag{3.4}$$

where m_{Tank} is the total mass in the tank, F_f is the total feed flow rate and x_{HD} is the mass fraction of heavy diesel. F_f / m_{Tank} represents the inverse of the time constant (τ_{tank}) of the tank and is estimated with real process measurements. Taking the Laplace transform of Eq. 3.4 with all variables are in deviation form we get:

$$(\tau_{Tank}\,s + 1)X_{HD,out} = X_{HD,in} \tag{3.5}$$

Rearranging Eq. 3.5, the mass balance becomes:

$$\frac{X_{HD,out}}{X_{HD,in}} = \frac{1}{(\tau_{Tank}\,s + 1)} \tag{3.6}$$

Taking the inverse laplace transform we get:

$$x_{HD,out} = x_{HD,in}(1 - e^{-t/\tau_{Tank}}) \tag{3.7}$$

Eg. 3.17 reveals the first order behavior of the blending model. Same equations can be written for each of the raw materials.

3.3 Estimation of Diesel Product's T^{95} Value

An important variable that is controlled in the plant is the T^{95} value of the diesel product obtained at the end of fractionation. The quality of Diesel is characterized by this value in the market. It is denoted by $Diesel\ T^{95}$ and it represents the boiling point at which 95% of diesel by volume boils. $Diesel\ T^{95}$ is estimated from the reactor product's normalized True Boiling Point (TBP) curve predicted by the reactor model. The normalized TBP curve is the plot of cumulative distilled mass fraction versus the normalized boiling point θ which is defined by:

$$\theta = \frac{TBP - \min(TBP)}{\max(TBP) - \min(TBP)} \tag{3.8}$$

The normalized TBP curve for the reactor product is given in Fig.3.7.a. along with the feed. It is seen that the product curve contains lower boiling point petroleum fractions than those fractions in the feed due to cracking. Diesel's TBP curve can be obtained from the TBP of the reactor product by using the temperature cut point (TCP) concept [34]. TCP is the point of demarcation between the lighter product naphta (to the left of TCP) and the heavier product diesel (to the right of TCP) which are separated from each other in the fractionation unit. The Diesel TBP curve is the portion of the product curve starting from the intersection of TCP with the product curve and is given in Fig.3.7.b. Once Diesel TBP curve is constructed, $Diesel\ T^{95}$ is estimated from the intersection of Diesel TBP curve with y=0.95 as shown in Fig 3.7.b. When the estimated values of $Diesel\ T^{95}$ were compared with the measured values, the average estimation error was found to be at an acceptable level of 1.4 K. The errors for five non-consecutive shifts are given in Table 3.3.

Table 3.3. *Diesel* T^{95} estimation errors.

Diesel T^{95} estimation	
AAD	1.4
RMSE	1.3
STD	0.070

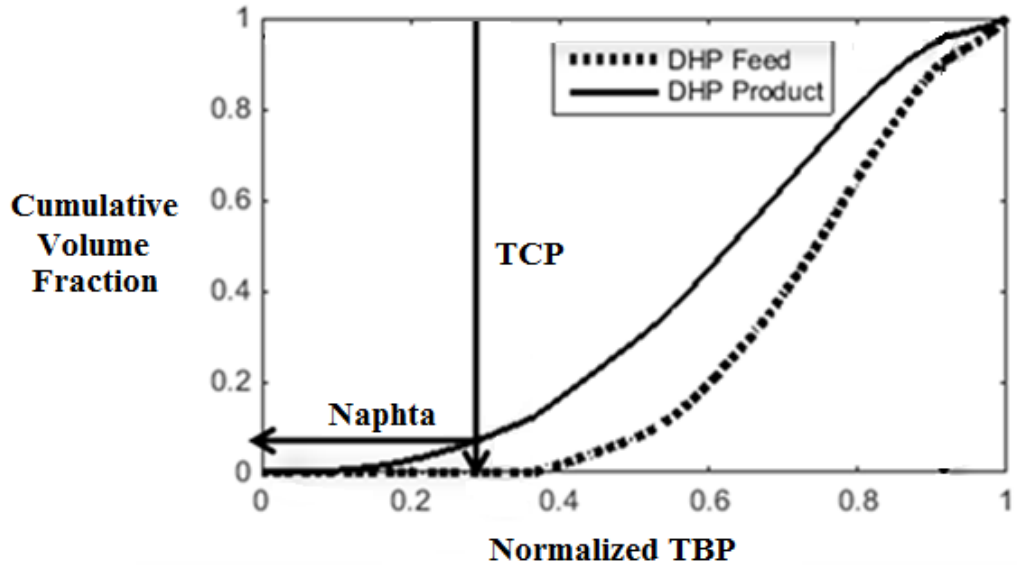

Figure 3.7.a. Construction of Diesel TBP curve using TCP.

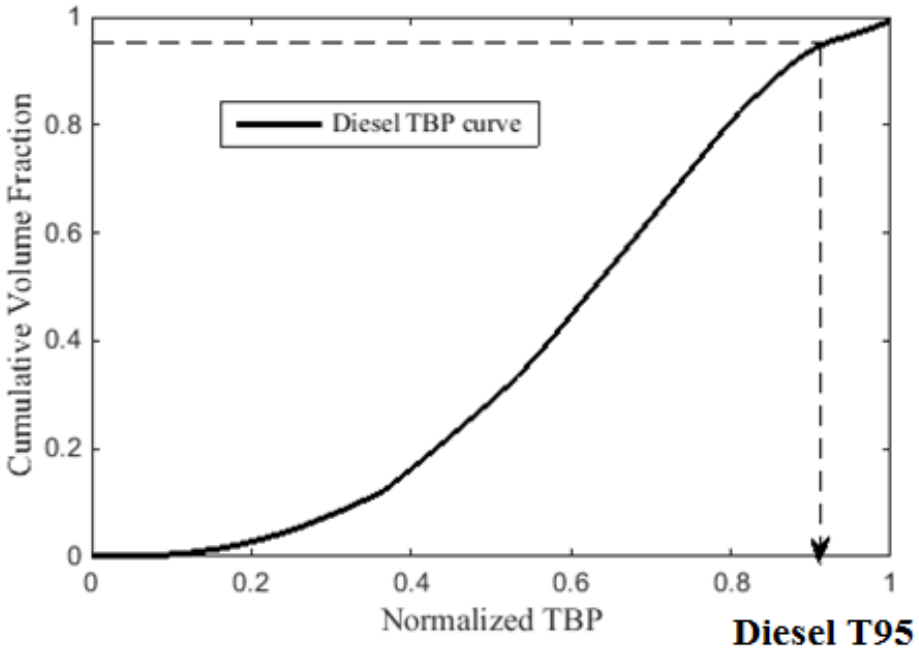

Figure 3.7.b. Calculation of *Diesel* T^{95}.

3.4 Hierarchical Model Predictive Control of the Diesel Hydroprocessing Plant

3.4.1 Hierarchical Cascaded MPC Structure

Model predictive controllers (MPC) have been extensively used in industrial applications lately [35]. The main idea of these controllers is to use a model to compute the optimal manipulated variables on-line while satisfying all the constraints. The algorithm estimates the disturbances, corrects the output predictions and calculates the optimal input moves by taking the process constraints into account. The idea is illustrated in Fig. 3.8. MPC computes the optimum control moves by minimizing the difference between the set-point and future predicted output values over a specified prediction horizon, N_p. During this optimization, the control moves are allowed to vary over a specified control horizon N_c. After the first optimal control move is implemented at sampling time *k*, the states and the outputs are updated using a Kalman Filter by the measurements available at the sampling time *k+1*. Following state estimation, the optimization and implementation cycle is repeated at time *k+1*. In this fashion, while MPC performs an open-loop optimization, it incorporates feedback information as well. For a review on the evolution of the model predictive controllers, the reader is referred to [36].

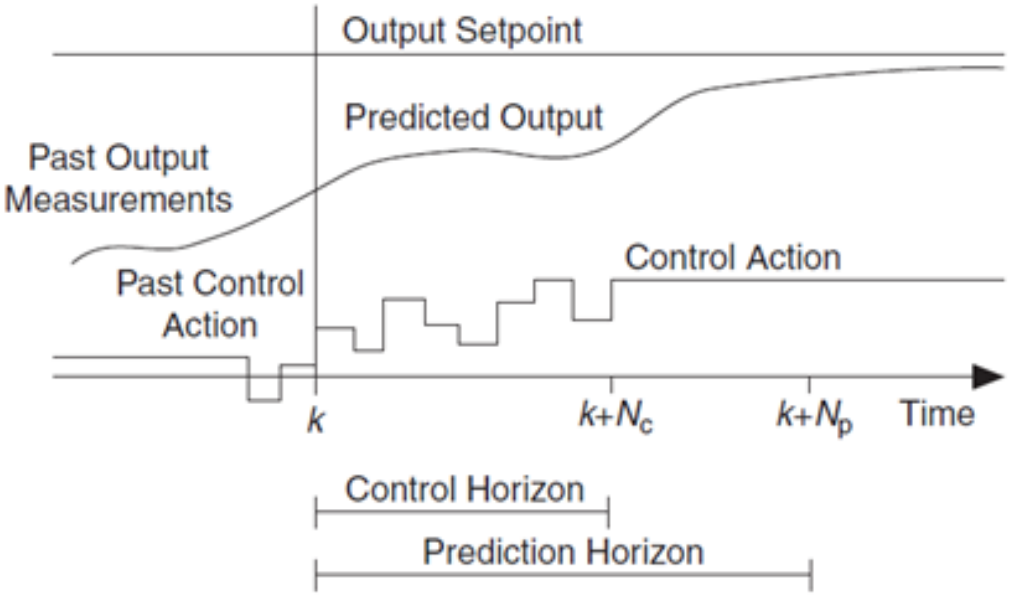

Figure 3.8. Model predictive control strategy.

Hierarchical model predictive controllers have a broad range of different application areas in literature. Falcone et al. [37] developed a hierarchical model predictive controller framework for autonomous vehicles. Vargas-Villamil and Rivera [38] presented a two layer approach for the real time optimization of reentrant manufacturing lines used for semiconductor manufacturing. The main objective was to maximize the production rate by using linear programming methods. Touretzky and Baldea [39] studied the benefits of two level model predictive controllers for minimizing the cooling energy demand of the residential buildings. Adetola and Guay [40] compared the advantages of single and two layer control approaches and designed a control system for uncertain non-linear processes. In a similar context, Ying and Joseph [41] developed a two stage approach to update the real time optimization set points for the Shell control problem. Sildir et al. [42] proposed a two level model predictive control configuration for the optimization and control of an industrial hydrocracking plant, in which a constant feed is processed by manipulating both reactor and separator operating conditions.

The DHP plant subject to this study has to run under the most profitable operating conditions while maintaining stability and not violating the operational constraints. In other words, the control system should address both economic and regulatory control objectives. It is well-known that the best way to organize and handle such different plant-wide control tasks is through hierarchical control [43], [44]. Therefore a hierarchical control structure is designed for the DHP Plant as shown in Figure 3.9. At the highest level of the hierarchy, the optimal steady-state operating points are calculated by performing an economic optimization. This optimization is usually performed by using a detailed, static nonlinear model of the system along with an economic objective function. Closed-loop control is performed by a cascade of MPCs. First, calculated optimum operating points are given to the supervisory layer model predictive controller. The supervisory MPC tracks the desired optimum operating points by adjusting the set-points of the outer loop control variables which represent the slower economic CVs. At the lower level, a regulatory MPC controls the inner loop controlled variables which are sampled much faster than the economic CVs.

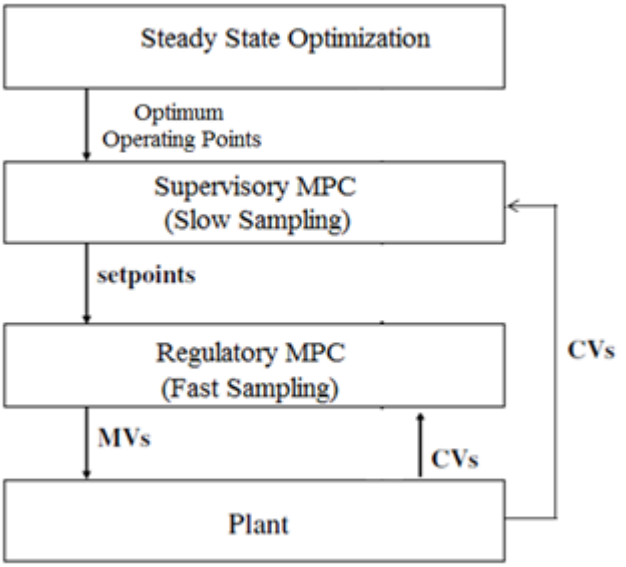

Figure 3.9. Hierarchical Control Structure.

3.4.2 Plant Wide Hierarchical Control of the DHP Plant

The DHP plant consists of the blending, hydro-desulfurization and fractionation subsystems as shown in Figure 3.10. Therefore, optimization should explore the joint profitability of all the subsystems and not violate the specified environmental and operational constraints. As shown in Fig. 3.10, the critical controlled variables (CVs) in the plant are the T95 value of the feed after blending ($Feed\ T^{95}$) and the reactor bed exit temperatures. These CVs are the most critical variables that affect the Diesel product's T95 value ($Diesel\ T^{95}$) and its sulfur content both of which have to meet the given specifications. Available manipulated variables (MVs) are the raw material flow-rates entering the blending unit and the hydrogen quench flow-rates that are adjusted by the PID controllers to control the reactor inlet temperatures.

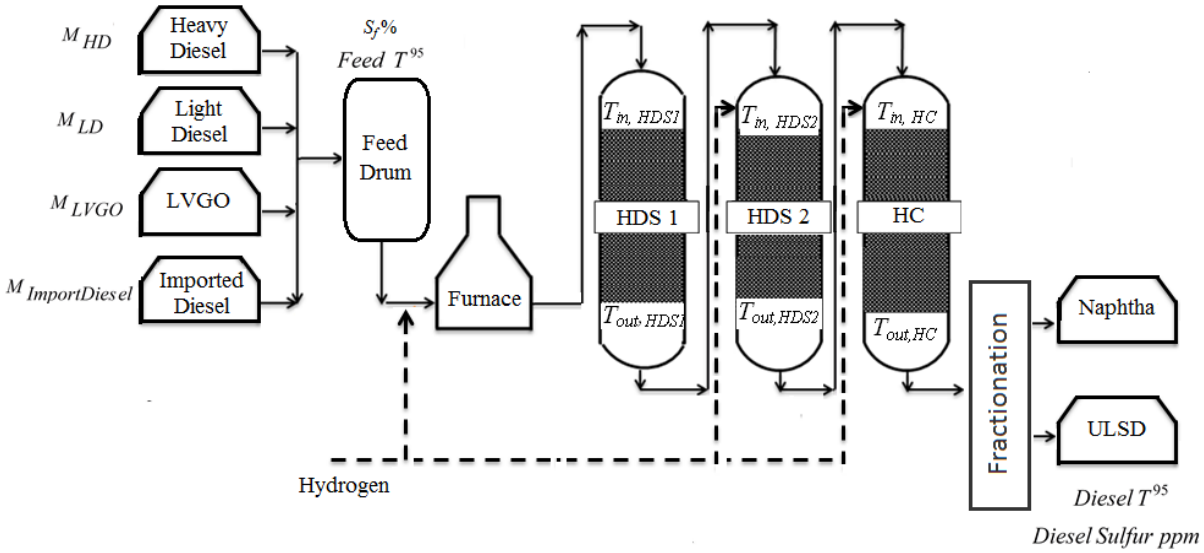

Figure 3.10. DHP Plant with the important MVs and CVs.

The effluent from the hydrocracker HC is sent to the fractionation unit where the main product Ultra-Low-Sulfur-Diesel (ULSD) is obtained. We assume that the fractionator's control system is able to maintain its desired operating conditions in response to different control actions taken by the upstream blending and reaction subsystems. This is a reasonable assumption based on the past plant operations. Therefore, only the fractionation product diesel properties are addressed here without a need for a detailed study of the fractionator's internal variables.

The hierarchical structure proposed for the DHP Plant is shown in detail in Fig. 3.11. The main task of this plant-wide MPC structure is to coordinate the local regulatory MPCs for the blending subsystem and the reactors to reach the plant wide optimal operating conditions. Each layer in the hierarchy has its own control task and algorithm as explained next.

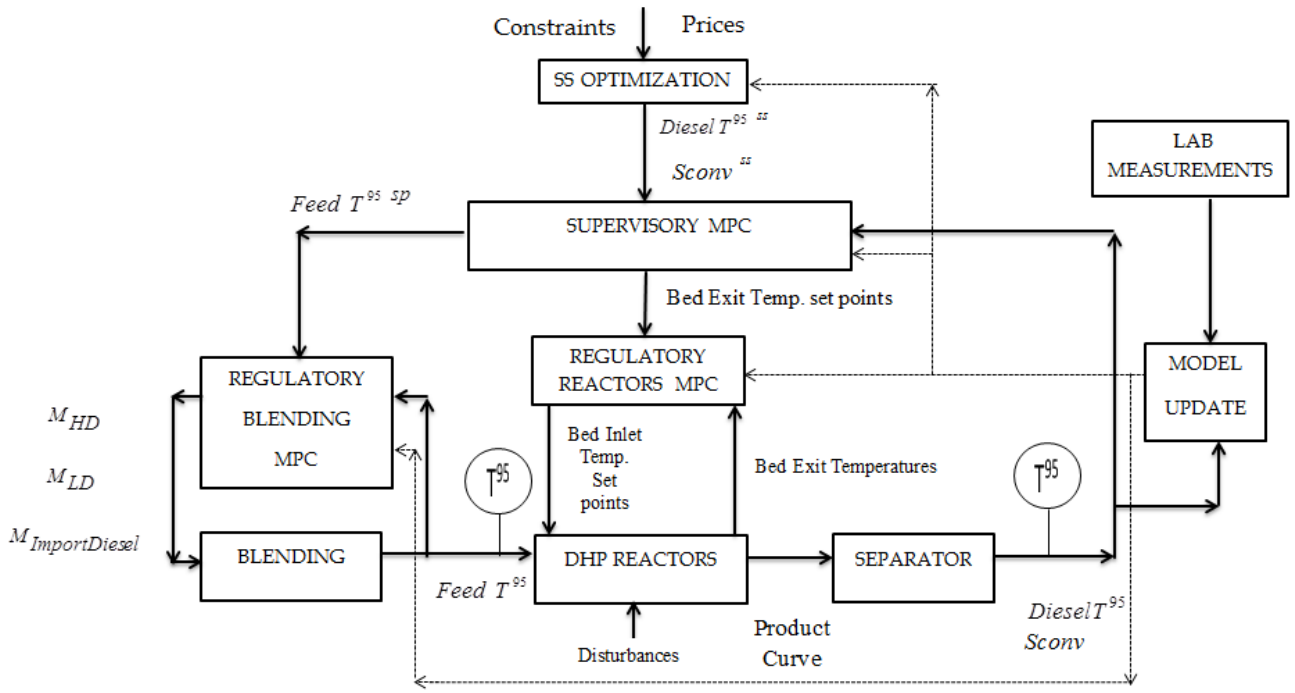

Figure 3.11. Plant Wide Control Structure of the DHP Plant.

3.4.2.1 Steady State Optimization

Steady-state optimization computes the optimal steady-state operating conditions by solving the following nonlinear constrained optimization problem:

$$\max_{u} \text{Profit} = P_{Diesel}M_{Diesel} + P_{Nafta}M_{Nafta} - C_{HD}M_{HD} - C_{LD}M_{LD} - C_{LVGO}M_{LVGO} - C_{ImportDiesel}M_{ImportDiesel}$$

s.t.

$$y = f_{ss}(u)$$

$$400 \le M_{HD} \le 600 \qquad 600 \le M_{LD} \le 800 \qquad 1300 \le M_{Im.Diesel} \le 1500$$

$$\Delta M_{LVGO} = 0 \qquad \Delta M_{HD} + \Delta M_{LD} + \Delta M_{Im.Diesel} = 0$$

$$-7 \le \Delta T_{in,HDS} \le 7\,K \qquad -7 \le \Delta T_{in,HC} \le 7\,K \tag{3.9}$$

$$T_{out,HC} < 655K \qquad T_{out,HDS1} < 655K \qquad T_{out,HDS2} < 655K$$

$$Sconv > 99.7\% \qquad 350\,^{0}C < DieselT^{95} < 360\,^{0}C \qquad 376\,^{0}C < FeedT^{95} 385\,^{0}C$$

$P_i's$ are the prices of the products and $C_i's$ are the costs of the raw materials, both of which are set by the refinery management. The refinery management also specifies the daily total flow rate of the unit. Utility cost is assumed to be constant since the total feed flow-rate is constant during the period of optimization.

The steady-state model f_{ss} represents the map between the decision variables *u* and outputs *y*. Decision variables *u* consist of the mass flow rates of the blended raw materials (ton/day) and the inlet temperatures of the reactors (K) i.e. $u = (M_{HD}, M_{LD}, M_{ImportDiesel}, T_{in,HDS1}, T_{in,HDS2}, T_{in,HC})$. Operational, safety and product constraints are specified in the form of equalities and inequalities. Equality constraints include the fact that LVGO is not allowed to change and the total feed flow-rate is kept constant. Inequality constraints include the restrictions on the flow-rates of the blended streams LD, HD and Import Diesel which are imposed by the upstream distillation column controllers; limits on the reactor bed exit temperatures; and the allowed changes in the inlet bed temperatures. Finally the main product Diesel must have its T^{95} value between 350 and 360 ^{o}C and its sulfur content must not exceed 10 ppm. After comparing the Diesel sulfur ppm measurements with sulfur conversions, it is realized that for conversion levels above 99.7%, the Diesel Sulfur never exceeds the limit of 10 ppm. Since it is very difficult to estimate the product sulfur amount at these low levels, we constrain the sulfur conversion instead ($Sconv > 99.7\%$), which is reliably predicted by the reactor model, to guarantee that diesel

sulfur content in ppm is below the specified limit. After comparing the Diesel sulfur ppm measurements with sulfur conversions obtained from plant measurements, it is realized that for conversion levels above 99.7%, the Diesel Sulfur never exceeds the limit of 10 ppm (see Fig. 3.12.) The sampling time of the optimization layer is one day. For long term economic disturbances like catalyst deactivation and feed quality changes, the nonlinear plant model should be recalibrated by re-estimating the model parameters when the prediction errors exceed certain threshold values and the steady-state optimization should use the updated model to determine the best operating conditions.

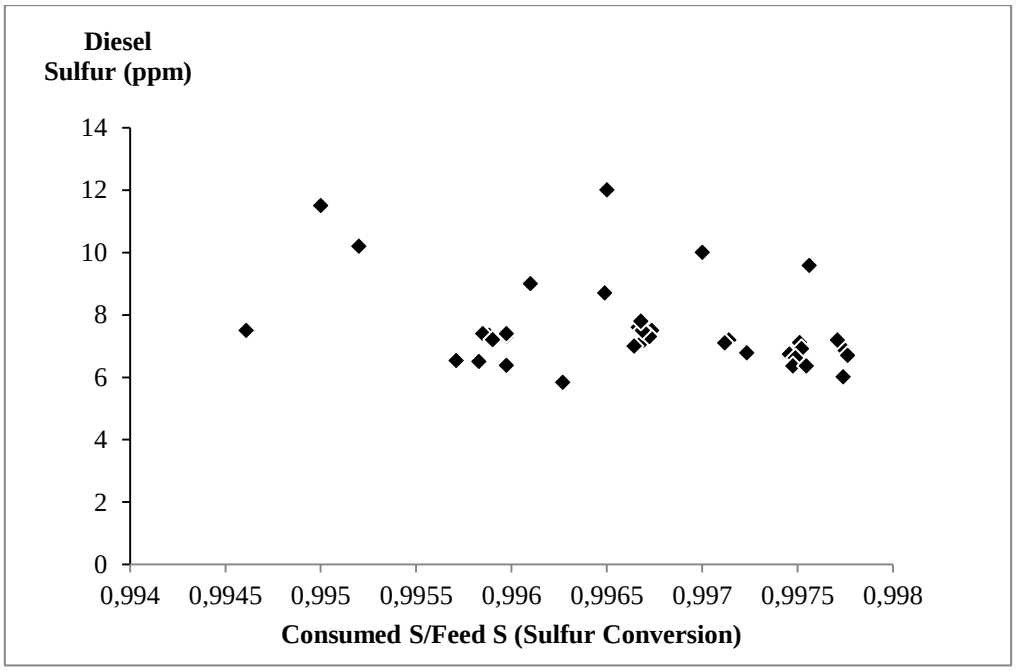

Figure 3.12. Diesel Sulfur ppm measurements with respect to sulfur conversions

3.4.2.2 Supervisory MPC

Below the steady state optimization is the hierarchical model predictive control system where economic decisions are converted to feedback implementations. At the top of this hierarchy, Supervisory MPC coordinates the local Regulatory Blending and the Reactor MPCs as shown in Fig. 3.11. Specifically, Supervisory MPC manipulates the set-point values of $Feed\ T^{95}$ and the set-point values of the exit temperatures of the reactor beds to meet the end product specifications ($Diesel\ T^{95}$ and *Sconv*).

Supervisory MPC uses the following linear state space model:

$$\begin{aligned} x(k+1) &= Ax(k) + B_u u(k) + B_d n_d(k) \\ y(k) &= Cx(k) + n_m(k) \end{aligned} \tag{3.10}$$

where *x* is the state vector including both the process and disturbance states. *u* and *y* are the vector of control inputs and outputs, respectively. n_d and n_m are white noises for the state and the measurements. Disturbances are modeled as integrated white noise and added to the controlled outputs to provide integral action [45], [46],[41]. In order to build the above model, step-changes in inputs $u = (Feed\ T^{95,sp}, T^{sp}_{out,HC}, T^{sp}_{out,HDS1}, T^{sp}_{out,HDS2})$ were made, and the nonlinear plant model was simulated under closed-loop conditions with the local regulatory MPCs, and the plant outputs $y = (Diesel\ T^{95}, S_{conv})$ were recorded. From this input-output data, the step-response model was obtained and converted to its linear state-space realization as in Eq. 3.10. Calculations were performed using MATLAB MPC Toolbox [47]. In these simulations the local MPCs were designed and tuned (see below) to give stable and smooth responses to the set-point changes made by the Supervisory MPC.

Supervisory MPC solves the following optimization problem at each sampling time *k* subject to the Eq. 3.11:

$$\min_{\Delta u(k|k),\ldots,\Delta u(k+M-1|k)} \sum_{i=0}^{P-1}\sum_{j=1}^{2} \left| w_{i+1,j}^{y}\left(y_j(k+i+1|k) - y_j^{ss}\right)\right|^2 + \sum_{j=1}^{4} \left| w_{i,j}^{\Delta u}\Delta u_j(k+i|k)\right|^2 + \sum_{j=1}^{4} \left| w_{i,j}^{u}\left(u_j(k+i|k) - u_j^{ss}\right)\right|^2 \tag{3.11}$$

s.t.

input constraints:

$$T_{out,HDS1}^{sp}(k+i|k) < 655\,K$$

$$T_{out,HDS2}^{sp}(k+i|k) < 655\,K$$

$$T_{HC}^{sp}(k+i|k) < 655\,K$$

$$376\ ^0C < Feed\ T^{95,sp}(k+i|k) < 385\ ^0C$$

output constraints:

$$Sconv(k+i|k) > 99.7\%$$

$$350\ ^0C < Diesel\ T^{95}(k+i|k) < 360\ ^0C$$

In the objective function the controlled outputs are $y = (Diesel\ T^{95}, S_{conv})$. These outputs are tracked close to their optimal steady-state values y^{ss} determined by the steady-state optimization. Optimization determines the optimal values of changes in the control inputs $u = (Feed\ T^{95,sp}, T_{out,HC}^{sp}, T_{out,HDS1}^{sp}, T_{out,HDS2}^{sp})$ which are supplied to the lower layer regulatory MPCs as optimal set-points. The last term in the objective function forces the inputs to their optimal steady state values u^{ss} determined by the steady-state optimization. The weights for the outputs, inputs and input changes are denoted by w^y, w^u and $w^{\Delta u}$; *P* is the prediction horizon and *M* is the number of control moves. Inequality constraints are used to keep the inputs and outputs within the operational limits and product specifications given by the plant management. Sampling period of the Supervisory MPC is 10 min which allows sufficient time for its changes to be implemented by the lower level regulatory controllers.

3.4.2.3 Regulatory MPCs

Regulatory MPCs are the decentralized model predictive controllers of the reactors (Regulatory Reactors MPC) and the blending unit (Regulatory Blending MPC). These controllers operate at a faster time scale than the Supervisory MPC with a sampling time 6 seconds to be able to reject fast disturbances and track the set-point changes.

Regulatory Reactors MPC controls the reactor exit temperatures at the desired set-points supplied by the Supervisory MPC. The available manipulated variables are the set-points of the reactor inlet temperatures. PID controllers (inside the DHP reactors block in Figure 3.11) are used to adjust the quench flows to control the reactor inlets at the set-points determined by Regulatory MPC. Regulatory Blending MPC tracks the set-point changes $Feed\ T^{95,sp}$ specified by the Supervisory MPC by manipulating the available raw material flow-rates of LD, HD and Import Diesel.

The models for both regulatory MPCs are derived in a similar fashion to the Supervisory MPC by step testing the first principles reactor model and the empirical blending model.

The objective function for each regulatory MPC is similar to Eq. 3.10. The particular inputs, outputs and the constraints used in each MPC design are summarized in Table 3.4.

Table 3.4. Inputs, outputs and constraints of regulatory MPCs.

	Regulatory Reactors MPC	Regulatory Blending MPC
Inputs	$T_{in,HDS1}^{sp}, T_{in,HDS2}^{sp}, T_{in,HC}^{sp}$	$M_{HD}, M_{LD}, M_{Im.Diesel}$
Outputs	$T_{out,HC}, T_{out,HDS1}, T_{out,HDS2}$	$Feed\ T^{95}$
Constraints	$-7 \le \Delta T^{sp}_{in,HDS1} \le 7\,K$ $-7 \le \Delta T^{sp}_{in,HDS2} \le 7\,K$ $-7 \le \Delta T^{sp}_{in,HC} \le 7\,K$ $T_{out,HC} < 655K$ $T_{out,HDS1} < 655K$ $T_{out,HDS2} < 655K$	$-200 \le \Delta M_{HD} \le 200$ $\quad -150 \le \Delta M_{LD} \le 150$ $0 = \Delta M_{LVGO}$ $\quad -200 \le \Delta M_{Im.Diesel} \le 200$ $\Delta M_{HD} + \Delta M_{LD} + \Delta M_{Im.Diesel} = 0$

The inlet temperatures of the reactor beds cannot be increased or decreased by more than 7 ^{0}C and the reactor exit temperatures cannot exceed their safety limits defined by the catalyst company. LVGO flowrate is not available for manipulation; changes in the other flows have upper and lower limits set by the upstream columns and the total flow-rate of the blended feed to the reactor is constant.

3.5 Results

3.5.1 Steady-state optimization

Initially, a nominal case was considered, where the plant operates at the steady state given as ‘BASE’ in Table 3.5. Next, steady state optimization Eq. 3.9 is solved and the optimum operating conditions are computed. Two different cases were considered. In the first case, the the blending unit was not optimized by keeping the raw material flow rates at their nominal values. Only the reactor operating conditions were optimized. The results are given under ‘OPTIMUM FOR A FIXED FEED’ in Table 3.5. In the second case, the optimum operating conditions for both the blending unit and reactors were computed. These results are also given in Table 3.5 as ‘OPTIMUM FOR A VARYING FEED’. Note that given process variables and simulation results were scaled with a constant for proprietary reasons.

Table 3.5. Steady-State Optimization Results*

	BASE	OPTIMUM FOR A FIXED FEED	OPTIMUM FOR A VARYING FEED
M_{HD} (ton/day)	495	495	600
M_{LD} (ton/day)	672	672	763.3
M_{LVGO} (ton/day)	240.6	240.6	240.6
$M_{Import\,Diesel}$ (ton/day)	1496.7	1496.7	1300
C_{HD}	1	1	1
C_{LD}	1.01	1.01	1.01
$C_{ImportDiesel}$	1.012	1.012	1.012
P_{Diesel}	1.05	1.05	1.05
P_{Nafta}	0.7	0.7	0.7
$T_{in1,HDS}$ (K)	626.6	627.4	627.3
$T_{in2,HDS}$ (K)	635.9	636.0	639.0
$T_{in,HC}$ (K)	613.4	608.0	609.9
$T_{out1,HDS}$ (K)	652.3	653.1	653.1
$T_{out2,HDS}$ (K)	649.7	652.5	653.2
$T_{out,HC}$ (K)	628.77	620.0	622.51
Bulk Feed Sulfur (%)	1.121	1.121	1.29
Sulfur Conversion (*Sconv*)	0.9959	0.997	0.997
Feed T^{95} (^{0}C)	380.9	380.9	382.4
Diesel T^{95} (^{0}C)	355.5	360	360
Diesel (ton/day)	2526	2580	2600
Profit (normalized)	1	2.117	2.23

*for proprietary reasons the numbers are scaled without distorting the general trends.

In both cases, optimization produces more and heavier diesel by increasing $Diesel\ T^{95}$ to its maximum allowed value of $360\ ^{0}C$. In the fixed feed case, the raw materials were not changed and the optimality was reached by decreasing only the hydrocracker exit temperature. Decreasing the hydrocracker exit temperature from 628.77 K to 620 K reduces the degree of hydrocracking, which in turn, increases $Diesel\ T^{95}$ value and the diesel production. The profit computed for this case was 2.117 times more than the base case.

In the varying feed case, both the blending and the reactor conditions were changed. The amount of HD used in the blend is increased to its maximum limit 600 ton/day since HD is the cheapest raw material. By the same reasoning, the import diesel which is the most expensive raw material is set to its lowest level of 1300 ton/day. However, the amount of LD is increased despite the fact that it is relatively expensive. This is due to the fact that the properties of LD (in terms of its TBP curve and T^{95} value) are closer to that of diesel product; thus, increasing LD increases diesel production, offsets the raw material cost and increases the net profit.

Under optimum operating conditions, the blended reactor feed gets heavier as shown by the increase in $Feed\ T^{95}$. This in turn helps to increase $Diesel\ T^{95}$ and the diesel production. Optimization also suggests decreasing the hydrocracker exit temperature. Decrease in reactor temperature reduces hydrocracking, which in turn, increases $Diesel\ T^{95}$ value and diesel production. However, the decrease in hydrocracker exit temperature was less than the fixed feed case from 628.77 K to 622.51 K. This is due to the fact that when the blend is adjusted, relatively less decrease in the hydrocracker temperature is required to increase $Diesel\ T^{95}$ and diesel production. In this case the overall profit increased with a factor of 2.23 which is higher than the fixed feed case as expected.

In the case of varying feed, the blended reactor feed gets heavier at the optimum conditions as shown by the increase in $Feed\ T^{95}$ from 380.9 ^{0}C to 382.4 ^{0}C. The feed sulfur level increases at the optimum conditions since the feed is heavier. Accordingly, optimization increases the inlet temperature of the HDS reactors in order to increase the sulfur removal. In fact the overall conversion after optimization reaches its minimum allowable level of 99.7 %.

3.5.2 Control

The main task of the control system is to maintain the plant at its economically optimum operating conditions. Therefore, the tracking performance of the controller was tested by moving the plant operation from the suboptimal base case to the optimal steady-state. At simulation time equal to 10 min, the controller was activated by making the changes recommended by steady-state optimization. Specifically, the varying feed case is considered and 4.5 ^{0}C step change in *Diesel* T^{95}, 1.5 ^{0}C step change in *Feed* T^{95} and 0.11 % step change in sulfur conversion were implemented. The closed-loop results are given in Figs. 3.13-3.15.

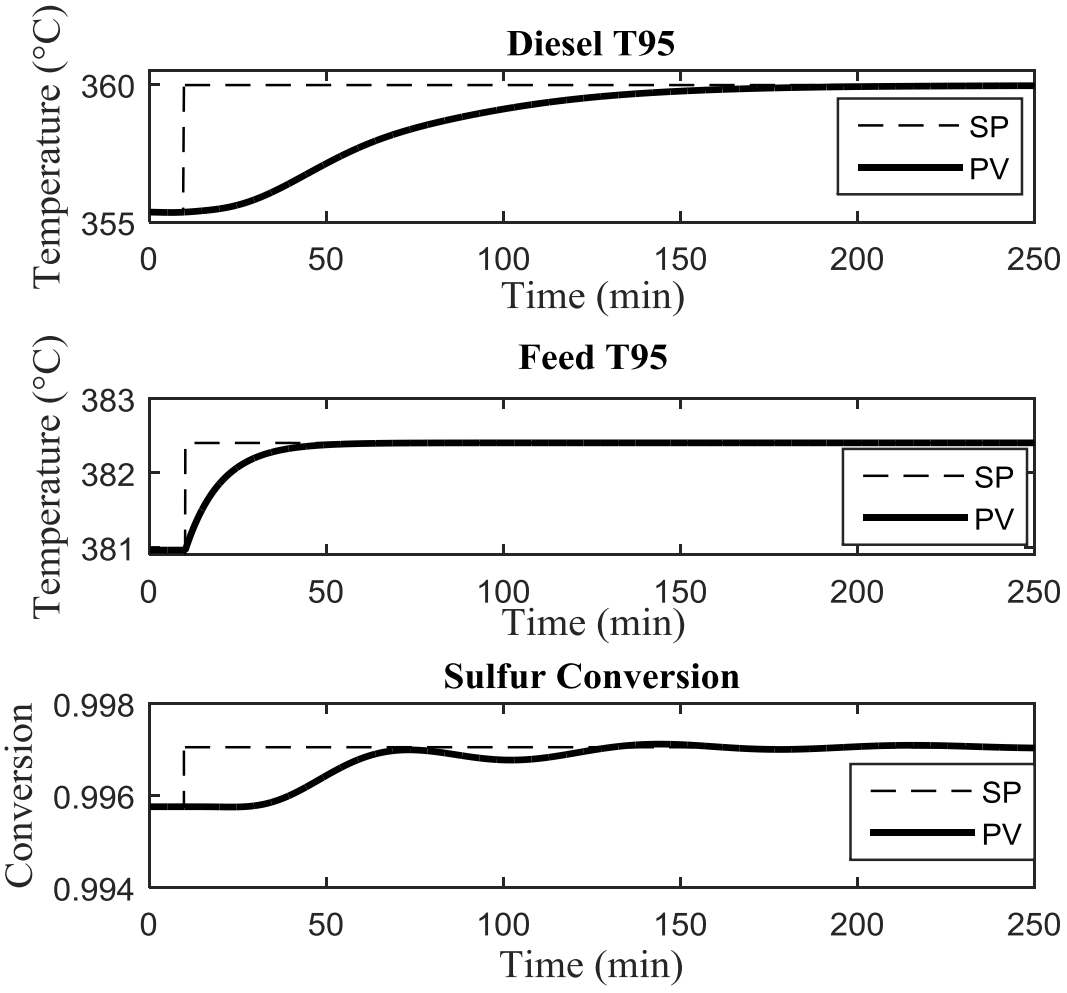

Figure 3.13. Tracking of the feed and product specifications.

Fig. 3.13 illustrates that the optimum steady-state operating conditions are obtained without any steady-state offset. *Diesel* T^{95} point and the sulfur level can be tracked in 150 minutes. The tuning parameters used in Supervisory MPC are listed in Table 3.6.

Fig. 3.14 shows the set-point change made in $Feed\ T^{95}$ by the Supervisory MPC and how this change is tracked by the Regulatory Blending MPC. In response to this set-point change, the raw material flow-rates HD, LD and Import Diesel are manipulated and $Feed\ T^{95}$ reaches its optimal value in 50 min. The tuning parameters used in regulatory MPCs are listed in Table 3.7.

Table 3.6. Supervisory Controller tuning parameters.

Sampling time	10 min					
P	9					
M	3					
Variables	$Feed\ T^{95,sp}$	$T^{sp}_{out,HDS1}$	$T^{sp}_{out,HDS2}$	$T^{sp}_{out,HC}$	$Diesel\ T^{95}$	$Sconv$
w^{y}	-	-	-	-	0.62	106
w^{u}	2.66	-	-	-	-	-
$w^{\Delta u}$	1.7	0.56	1.35	2.25	-	-

Table 3.7. Regulatory Controllers tuning parameters.

Sampling time	0.1 min						
P	70						
M	2						
Variables	$T_{out,HDS1}$	$T_{out,HDS2}$	$T_{out,HC}$	$T_{in,HDS1}^{sp}$	$T_{in,HDS2}^{sp}$	$T_{in,HC}^{sp}$	$Feed\ T^{95}$
w^{y}	0.11	0.11	0.17	-	-	-	1
w^{u}	-	-	-	0.1	-	-	-
$w^{\Delta u}$	-	-	-	4.2	4.2	4.7	-

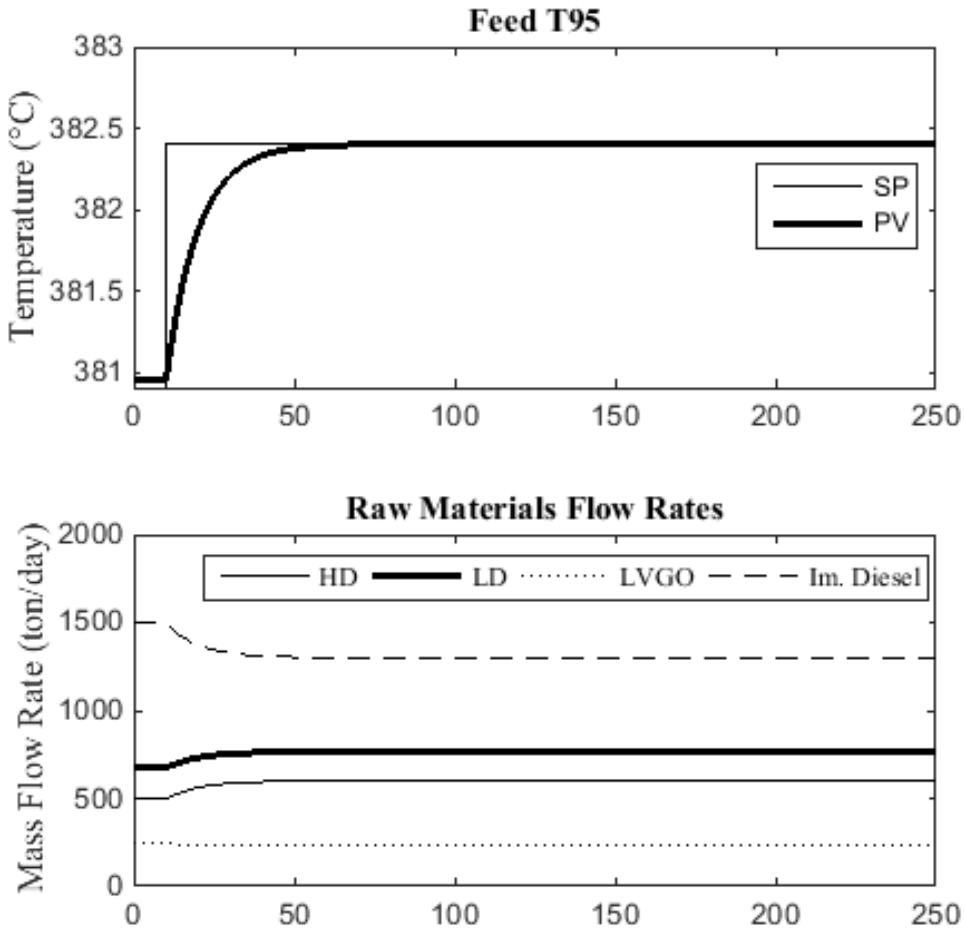

Figure 3.14. Closed-loop responses of the Regulatory Blending MPC layer.

When the feed sulfur content increases as a result of the changes made in the raw material flow rates by the Blending MPC, the Supervisory MPC demands higher set-points for both HDS exit temperatures to remove more sulfur as shown in Fig. 3.15. In return, the Regulatory Reactors MPC increases the inlet temperatures of the HDS. It is seen that exit HDS temperatures are able to track the optimal set-point changes. In the meantime, the set-point of the hydrocracker exit temperature is decreased in order to increase $Diesel\,T^{95}$. Since the non-linearity in the hydrocracking reactor is higher than that of the hydro-desulfurization reactors, MPC avoids large set point changes for HC and tracks a sequence of smaller set-point changes towards the final steady-state optimum. Contrary to HC, MPC implements single set-point changes in the HDS reactors.

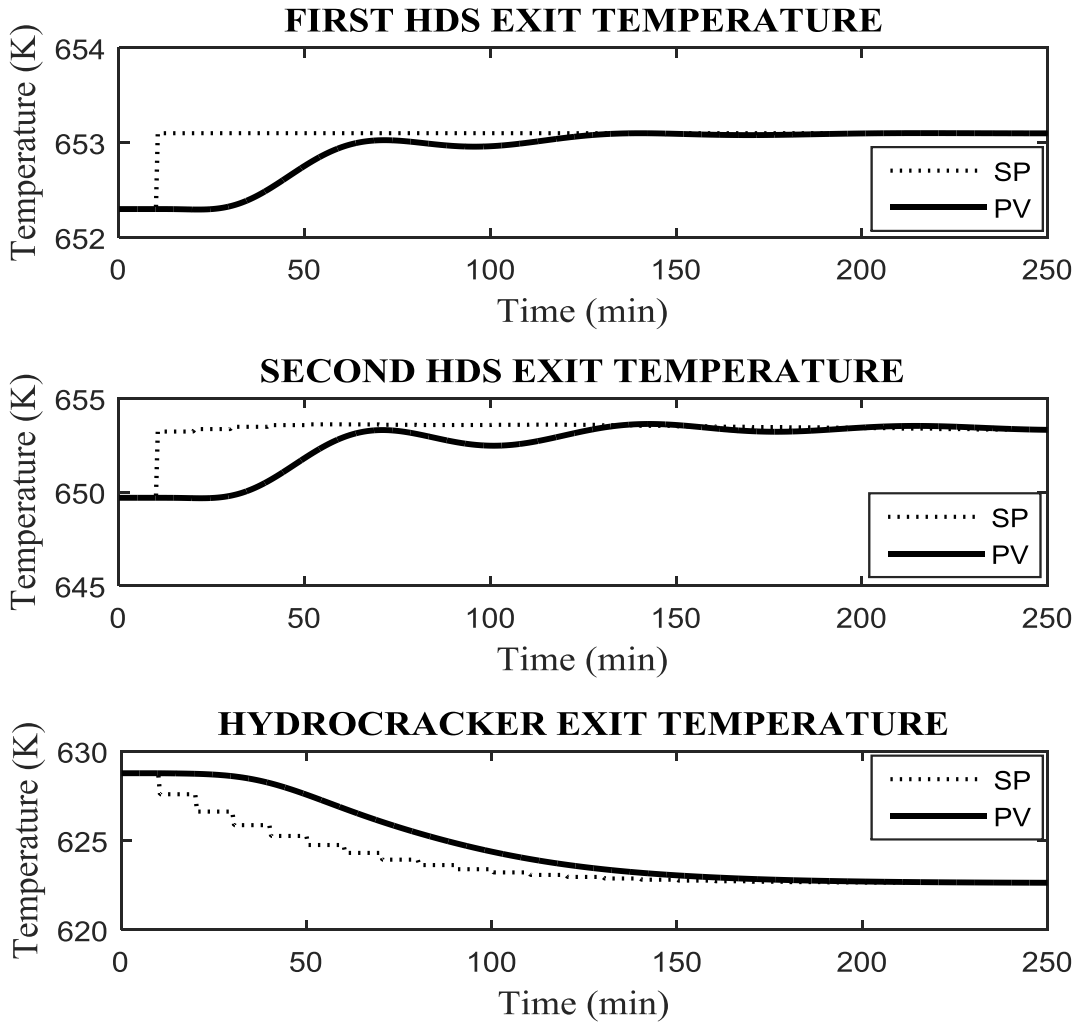

Figure 3.15. Closed loop responses of the reactor bed exit temperatures.

Next we consider the case that the refinery management demands an operation with a fixed reactor charge. This is the case defined as “fixed feed” in Table 5. Here the product specifications must be controlled by the reactor bed exit temperatures only. The results are given in Fig. 3.16 and Fig. 3.17.

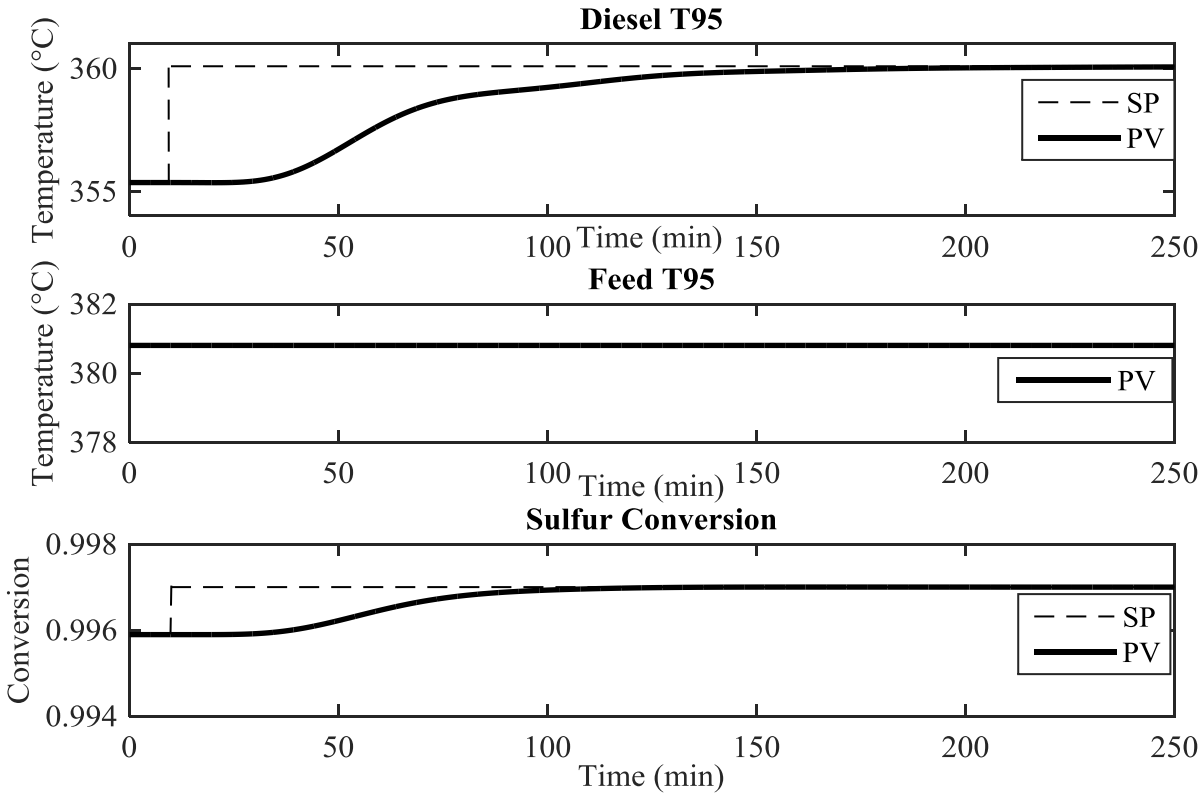

Figure 3.16. Closed loop responses of product specifications for a fixed feed blend.

Diesel T^{95} point reaches the optimal value slightly (about 7 min) than the varying feed case since *Feed* T^{95} is no longer available for manipulation. In order to increase *Diesel* T^{95}, the controller decreases the exit temperature of the hydrocracker bed by 2.5 ^{0}C more (compared to the varying feed case) and tracks it well. The sulfur conversion level was tracked faster as well since the high sulfur containing raw material flow rates were not increased. The bulk sulfur content of the feed is 1.121 % which is lower than the varying feed's sulfur content of 1.29%. As a result, the controller is able to track the desired sulfur conversion by making smaller set-point changes in the HDS reactor temperatures.

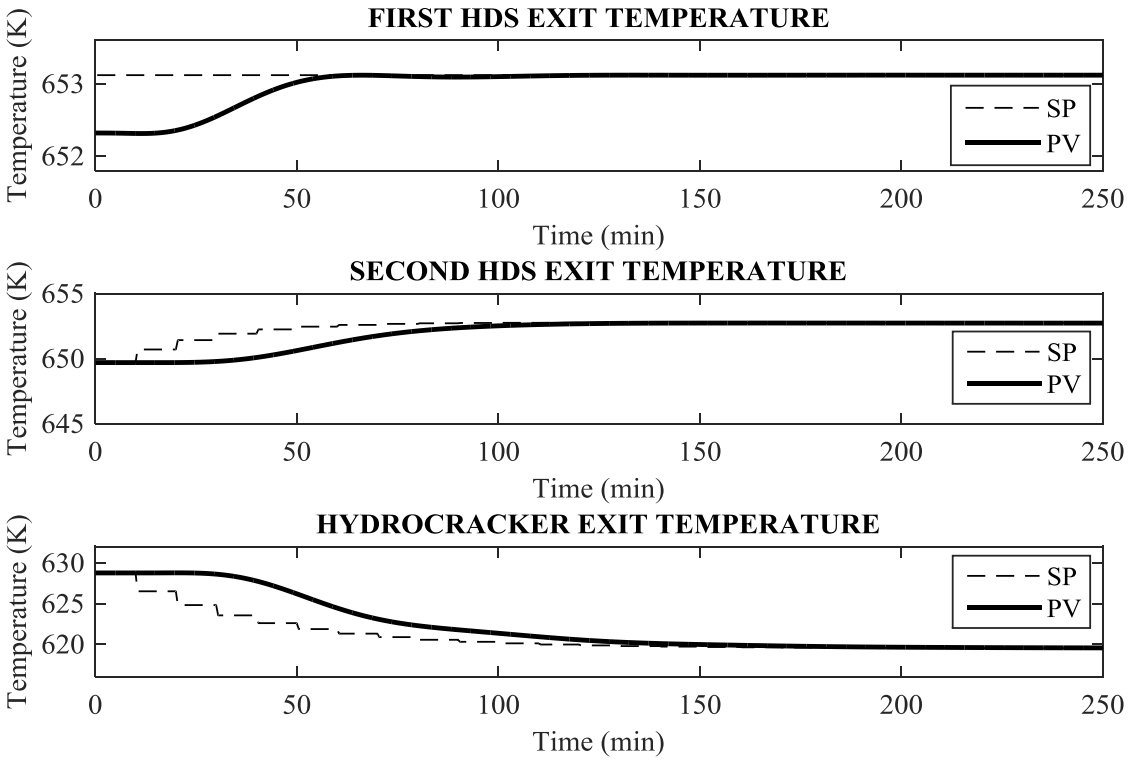

Figure 3.17. Closed loop responses of the reactor bed exit temperatures for a fixed feed blend.

Finally, we checked the disturbance rejection performance of the controller. After the plant was tracked to the optimum steady state operating conditions, at t=200 min, the ASTM D86 characteristics of heavy diesel feed was instantaneously changed as shown in Fig. 3.18, and heavy diesel became heavier. This increase resulted in an increase on the number of higher boiling point petroleum fractions in the feed. As a result, the $Feed\ T^{95}$ value increased to 382.8 ^{0}C. Corresponding control decisions for rejecting the disturbance are given in Figs 3.19-3.21.

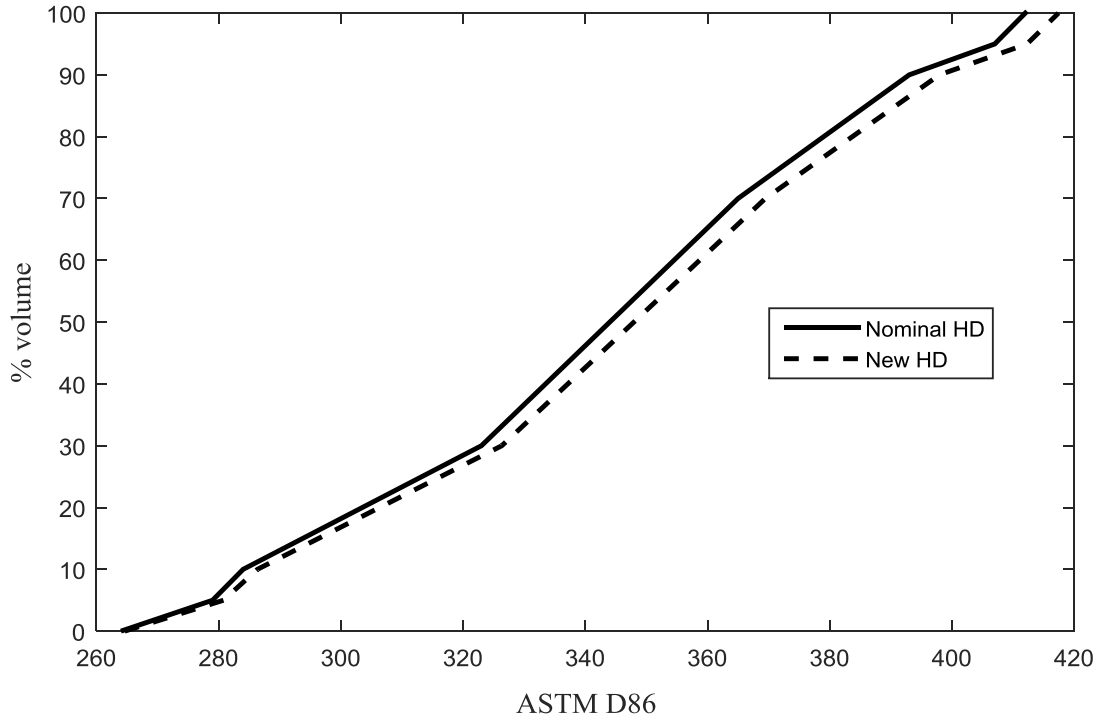

Figure 3.18. Heavy Diesel (HD) D86 values before and after the disturbance.

As shown in Fig. 3.19, the regulatory blending controller decreases the light diesel (LD) and heavy diesel (HD) flow rates, which are relatively higher than import diesel, to reject the increase on $Feed\ T^{95}$. Accordingly, $Feed\ T^{95}$ value is returned back to its optimum value of 382.4 ^{0}C. Meanwhile, Import Diesel flow rate is increased to keep the total feed flow-rate constant. Since the higher boiling point petroleum fractions introduced by the heavier feed crack more easily [30], the reactor effluent consists of more of the lighter fractions than diesel; therefore, $Diesel\ T^{95}$ temporarily decreases from 360 to 359.6 ^{0}C as shown in Fig. 3.20. In addition, the decrease in LD and HD flow-rates also contribute to the decrease in $Diesel\ T^{95}$.

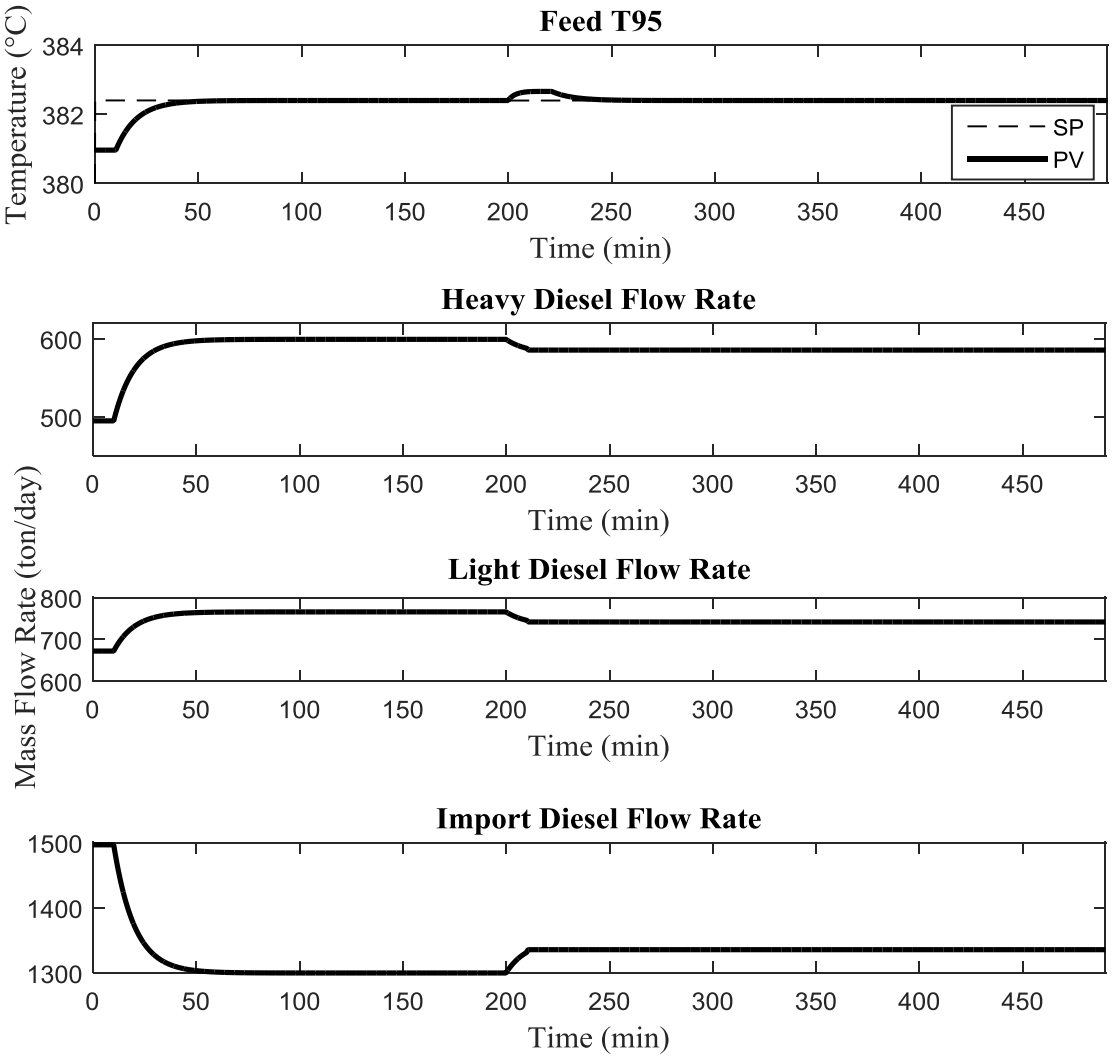

Figure 3.19. Responses of raw material flow rates in the presence of feed disturbance.

As shown in Fig. 3.21, the Reactor MPC decreases the hydrocracker reactor exit temperature by 0.8 ^{0}C to increase $Diesel\,T^{95}$ back to its original set-point value. The increase on $Feed\,T^{95}$ did not affect the sulfur conversion level significantly; therefore, the controller did not give considerable set point changes to the exit temperatures of hydro-desulfurization reactors.

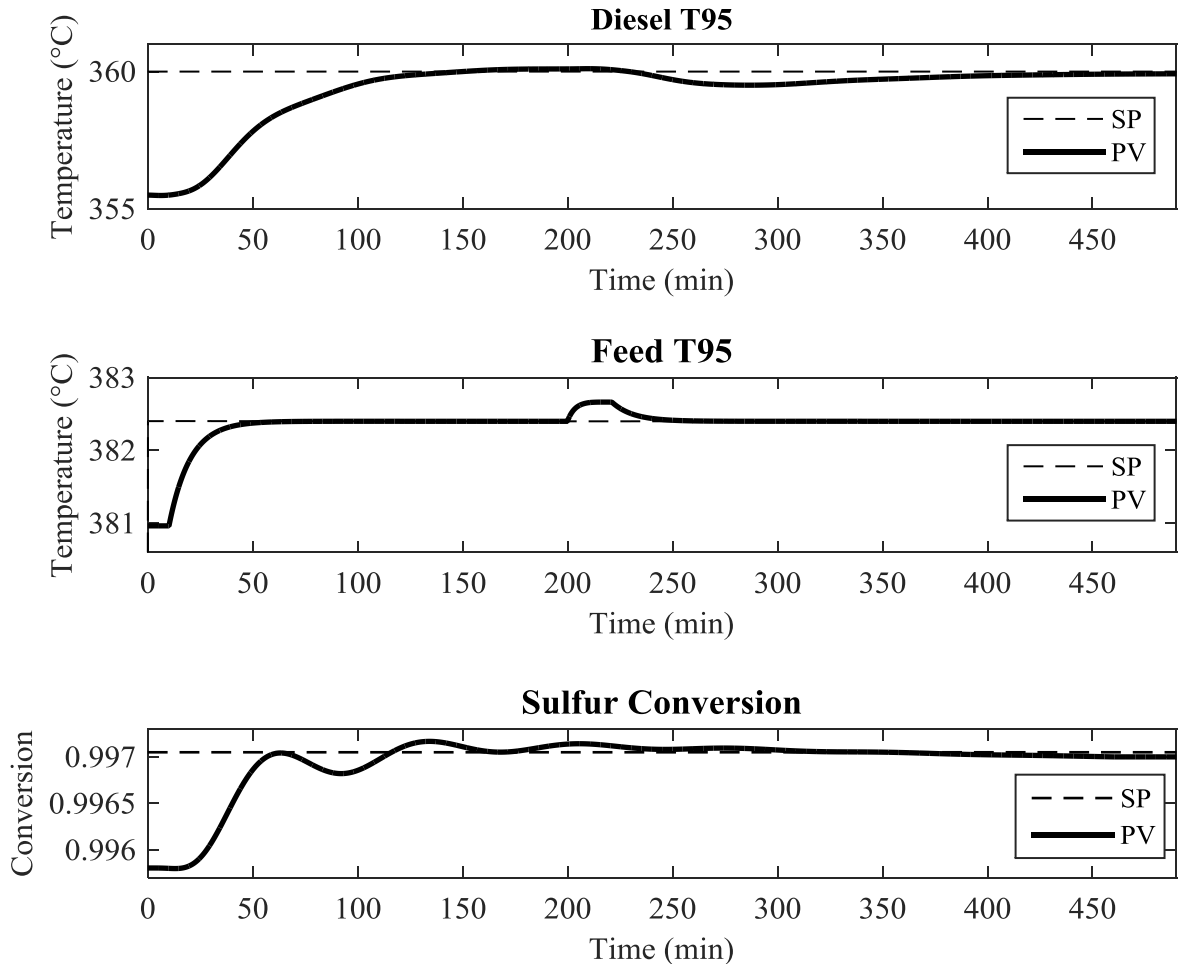

Figure 3.20. Response of product specifications and $Feed\ T^{95}$ to the feed disturbance.

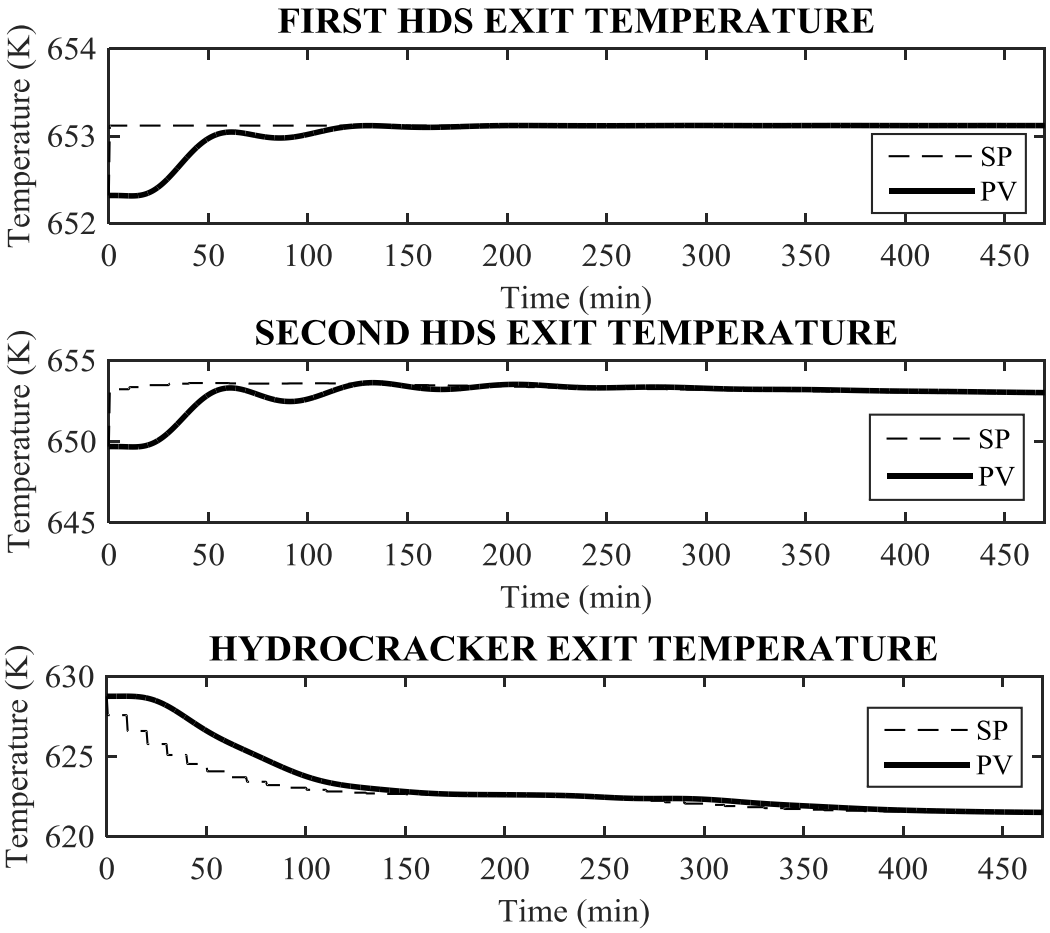

Figure 3.21. Responses of exit bed temperatures in the presence of feed disturbance.

Chapter 4

CONCLUSIONS

As the modeling scope of this thesis, a single-phase, pseudo-homogeneous and one dimensional dynamic reactor model was developed for the industrial diesel hydroprocessing plant of a refinery. The overall plant model consists of an HDS model for the first two hydrodesulfurization beds followed by an HC model for the last cracking bed. For both HDS and HC reactors, kinetics were modeled using the continuous lumping method. Critical model parameters were determined using parameter estimation techniques and real plant data. Simulations show that the model outputs are in excellent agreement with real plant data for both steady and dynamic cases. The maximum average absolute error for the prediction of temperatures is below 0.3 ^{0}C. Moreover, sulfur consumption rate and Diesel T95 are predicted with less than 8 kg/day and 2.6 ^{0}C absolute errors, respectively.

In the optimization and control part, the interest is in the use of the proposed models for optimizing the plant operating conditions and designing model predictive controllers for this industrial plant. A hierarchical structure is developed for plant-wide optimization and control of an industrial diesel hydro-processing (DHP) plant that consists of a blending unit for the feed, two catalytic hydro-desulfurization (HDS) reactor beds, one hydro-cracking (HC) reactor bed and a fractionation unit in series. For both reactors we make use of the first principles models we have developed earlier. For the feed blending and the fractionation units, we present new empirical models to predict certain important properties of the feed and product for optimization and control purposes. These include sulfur content of the feed, D86 curve of the feed and T^{95} value of the diesel product. A cascaded MPC structure is used to implement the results of steady-state optimization. In particular a Supervisory MPC coordinates the local blending and reactor MPCs by specifying the set-points of their CVs. Different simulation scenarios show that the plant can track the steady-state optimal operating conditions for the critical process variables such as T^{95} value of the feed and diesel product,

the exit temperatures of the reactor beds and sulfur removal while maintaining the plant within its safety and operational constraints.

After this study, the potential benefits of the proposed real time optimization scheme have been found significant. Thus, the research and development center and the refinery management are currently in the process of implementing the proposed optimization and control structure along with the process models to the industrial diesel hydro-processing plant.

BIBLIOGRAPHY

[1] A. Stanislaus, A. Marafi, M.S. Rana, Recent advances in the science and technology of ultra low sulfur diesel (ULSD) production, Catalysis Today, 153 (2010) 1-68.
[2] L.H. R.E. Palmer, S.Thakkar, S.Polcar, P.H.Desa, Design considerations for ULSD Hydrotreaters, NPRA 2003 Annual Meeting, (2003).
[3] J. Ancheyta, Modeling of Catalytic Hydrotreating, Modeling and Simulation of Catalytic Reactors for Petroleum Refining, John Wiley & Sons Inc2011, pp. 211-312.
[4] C. Song, An overview of new approaches to deep desulfurization for ultra-clean gasoline, diesel fuel and jet fuel, Catalysis Today, 86 (2003) 211-263.
[5] A. Gruia, Hydrotreating, in: D.J.S. Jones, P. Pujadó (Eds.) Handbook of Petroleum Processing, Springer, Netherlands, 2006, pp. 321-354.
[6] R. Aris, G.R. Gavalas, On the Theory of Reactions in Continuous Mixtures, 1966.
[7] M.Y. Chou, T.C. Ho, Continuum theory for lumping nonlinear reactions, AIChE Journal, 34 (1988) 1519-1527.
[8] I. Elizalde, J. Ancheyta, Modeling the Simultaneous Hydrodesulfurization and Hydrocracking of Heavy Residue Oil by using the Continuous Kinetic Lumping Approach, Energy & Fuels, 26 (2012) 1999-2004.
[9] M. Sau, C.S.L. Narasimhan, R.P. Verma, A Kinetic model for hydrodesulfurisation, in: B.D. G.F. Froment, P. Grange (Eds.) Studies in Surface Science and Catalysis, Elsevier1997, pp. 421-435.
[10] G.F. Froment, G.A. Depauw, V. Vanrysselberghe, Kinetic modeling and reactor simulation in hydrodesulfurization of oil fractions, Industrial & engineering chemistry research, 33 (1994) 2975-2988.
[11] H. Korsten, U. Hoffmann, Three-phase reactor model for hydrotreating in pilot trickle-bed reactors, AIChE Journal, 42 (1996) 1350-1360.
[12] M. Bhaskar, G. Valavarasu, B. Sairam, K.S. Balaraman, K. Balu, Three-phase reactor model to simulate the performance of pilot-plant and industrial trickle-bed reactors sustaining hydrotreating reactions, Industrial & Engineering Chemistry Research, 43 (2004) 6654-6669.
[13] R. Chowdhury, E. Pedernera, R. Reimert, Trickle-bed reactor model for desulfurization and dearomatization of diesel, AIChE Journal, 48 (2002) 126-135.
[14] M. Sau, C.S.L. Narasimhan, R.P. Verma, A Kinetic model for hydrodesulfurisation, in: B.D. G.F. Froment, P. Grange (Eds.) Studies in Surface Science and Catalysis, Elsevier1997, pp. 421-435.
[15] K. Basak, M. Sau, U. Manna, R.P. Verma, Industrial hydrocracker model based on novel continuum lumping approach for optimization in petroleum refinery, Catalysis Today, 98 (2004) 253-264.
[16] K. Sertić-Bionda, Z. Gomzi, T. Šarić, Testing of hydrodesulfurization process in small trickle-bed reactor, Chemical Engineering Journal, 106 (2005) 105-110.
[17] P. Mahinsa, M.T. Sadegh, H. Ganji, S. Shokri, Two Dimensional Dynamic Modeling of Hydrodesulphurization Reactor, Journal of Petroleum Science Research, 1 (2012).
[18] F.S. Mederos, M.A. Rodríguez, J. Ancheyta, E. Arce, Dynamic Modeling and Simulation of Catalytic Hydrotreating Reactors, Energy & Fuels, 20 (2006) 936-945.
[19] F.S. Mederos, J. Ancheyta, I. Elizalde, Dynamic modeling and simulation of hydrotreating of gas oil obtained from heavy crude oil, Applied Catalysis A: General, 425–426 (2012) 13-27.
[20] M.A. Hastaoglu, B.E. Jibril, Transient modeling of hydrodesulfurization in a fixed-bed reactor, Chemical Engineering Communications, 190 (2003) 151-170.

[21] J. Chen, Z. Ring, T. Dabros, Modeling and Simulation of a Fixed-Bed Pilot-Plant Hydrotreater, Industrial & Engineering Chemistry Research, 40 (2001) 3294-3300.
[22] H. Sildir, Y. Arkun, B. Cakal, D. Gokce, E. Kuzu, A dynamic non-isothermal model for a hydrocracking reactor: Model development by the method of continuous lumping and application to an industrial unit, Journal of Process Control, 22 (2012) 1956-1965.
[23] M. Riazi, Characterization and properties of petroleum fractions, ASTM international West Conshohocken, PA2005.
[24] G.C. Goodwin, R.L. Payne, Dynamic System Identification: Experiment Design and Data Analysis, Academic Press1977.
[25] K. Schittkowski, Experimental design tools for ordinary and algebraic differential equations, Industrial & Engineering Chemistry Research, 46 (2007) 9137-9147.
[26] S.A. Ali, Thermodynamic Aspects of Hydrodesulfurization and Hydrodenitrogenation, Petroleum Science and Technology, 25 (2007) 841-852.
[27] M.J. Girgis, B.C. Gates, Reactivities, reaction networks, and kinetics in high-pressure catalytic hydroprocessing, Industrial & Engineering Chemistry Research, 30 (1991) 2021-2058.
[28] C.G. Ma, H.X. Weng, A Study on the Lumping Kinetic Model for a Residual Oil Hydrodesulfurization Process, Energy Sources, Part A: Recovery, Utilization, and Environmental Effects, 34 (2012) 1933-1942.
[29] J. Ancheyta, S. Sánchez, M.A. Rodríguez, Kinetic modeling of hydrocracking of heavy oil fractions: A review, Catalysis Today, 109 (2005) 76-92.
[30] C.S. Laxminarasimhan, R.P. Verma, P.A. Ramachandran, Continuous lumping model for simulation of hydrocracking, AIChE Journal, 42 (1996) 2645-2653.
[31] H.J. Martinez-Grimaldo, J.C. Chavarria-Hernandez, J. Ramirez, R. Cuevas, H. Ortiz-Moreno, Prediction of sulfur content, API gravity, and viscosity using a continuous mixture kinetic model for Maya crude oil hydrocracking in a slurry-phase reactor, Energy & Fuels, 25 (2011) 3605-3614.
[32] W. Li, C.-W. Hui, A. Li, Integrating CDU, FCC and product blending models into refinery planning, Computers & Chemical Engineering, 29 (2005) 2010-2028.
[33] J.C. Morud, S. Skogestad, Analysis of instability in an industrial ammonia reactor, AIChE Journal, 44 (1998) 888-895.
[34] E. Aydın, A.D. Celebi, H. Sildir, Y. Arkun, U. Canan, G. Is, M. Erdogan, Dynamic modeling of an industrial diesel hydroprocessing plant by the method of continuous lumping, Computers & Chemical Engineering, 82 (2015) 44-54.
[35] S.J. Qin, T.A. Badgwell, A survey of industrial model predictive control technology, Control Engineering Practice, 11 (2003) 733-764.
[36] M. Morari, J. H. Lee, Model predictive control: past, present and future, Computers & Chemical Engineering, 23 (1999) 667-682.
[37] P. Falcone, F. Borrelli, H.E. Tsengz, J. Asgari, D. Hrovat, A hierarchical Model Predictive Control framework for autonomous ground vehicles, American Control Conference, 2008, 2008, pp. 3719-3724.
[38] F.D. Vargas-Villamil, D.E. Rivera, A model predictive control approach for real-time optimization of reentrant manufacturing lines, Computers in Industry, 45 (2001) 45-57.
[39] C.R. Touretzky, M. Baldea, Integrating scheduling and control for economic MPC of buildings with energy storage, Journal of Process Control, 24 (2014) 1292-1300.
[40] V. Adetola, M. Guay, Integration of real-time optimization and model predictive control, Journal of Process Control, 20 (2010) 125-133.
[41] C.-M. Ying, B. Joseph, Performance and stability analysis of LP-MPC and QP-MPC cascade control systems, AIChE Journal, 45 (1999) 1521-1534.

[42] H. Sildir, Y. Arkun, B. Cakal, D. Gokce, E. Kuzu, Plant-wide hierarchical optimization and control of an industrial hydrocracking process, Journal of Process Control, 23 (2013) 1229-1240.
[43] M. Morari, Y. Arkun, G. Stephanopoulos, Studies in the synthesis of control structures for chemical processes: Part I: Formulation of the problem. Process decomposition and the classification of the control tasks. Analysis of the optimizing control structures, AIChE Journal, 26 (1980) 220-232.
[44] R. Scattolini, Architectures for distributed and hierarchical model predictive control–a review, Journal of Process Control, 19 (2009) 723-731.
[45] K.R. Muske, T.A. Badgwell, Disturbance modeling for offset-free linear model predictive control, Journal of Process Control, 12 (2002) 617-632.
[46] U. Maeder, F. Borrelli, M. Morari, Linear offset-free Model Predictive Control, Automatica, 45 (2009) 2214-2222.
[47] A. Bemporad, M. Morari, N.L. Ricker, Model Predictive Control Toolbox 3 User's Guide, The mathworks, (2010).